Solid State Reactions Involving Oxides of Trivalent Cations

S. J. Schneider, R. S. Roth, and J. L. Waring

(April 11, 1961)

Selected mixtures in 69 binary systems involving Al_2O_3, Ga_2O_3, Cr_2O_3, Fe_2O_3, Sc_2O_3, In_2O_3, Y_2O_3, and the rare earth oxides were studied by X-ray diffraction techniques after heat treatment at various temperatures. A plot of the radii of the A^{+3} cations versus the radii of B^{+3} cations shows the regions of stability for the different structure types found for the double oxides of the trivalent cations. The following structure types were encountered: A, B, and C-type rare earth oxide; corundum, beta gallia; kappa alumina; garnet; perovskite; and several types which could not be definitely related to known structures. The majority of $A^{+3}B^{+3}O_3$ compounds have the perovskite structure. Several phases, including $(1-x)Fe_2O_3 \cdot xAl_2O_3$ ss and $(1-x)Fe_2O_3 \cdot xGa_2O_3$ ss, appear to have structures similar to kappa alumina. Solid solution definitely occurs in many of the garnet type compounds which contain gallia. Based on the data collected in this survey, the subsolidus phase equilibria relationships of 79 binary systems were drawn.

1. Introduction

In the field of phase equilibria research it is often beneficial to first survey a series of related systems before commencing on a detailed analysis of specific systems. A survey was recently conducted by the authors [1][^1] on the various solid state reactions that occur in mixtures of the trivalent rare earth oxides. It was found in the work that ionic size was the primary controlling factor in determining the various subsolidus phase relationships. This study has since been extended to include the oxides of the smaller trivalent cations, In^{+3}, Sc^{+3}, Fe^{+3}, Cr^{+3}, Ga^{+3}, and Al^{+3}. These cations, together with the lanthanide series comprise almost the entire group of ions which are commonly trivalent.

To date, only a limited number of binary oxide systems involving only trivalent cations have been completely studied. With the exception of the previously mentioned paper by Schneider and Roth [1], most of the research has been concerned with studies of $A^{+3}B^{+3}O_3$ and to a lesser extent $A_3^{+3}B_5^{+3}O_{12}$ type compounds. The $A^{+3}B^{+3}O_3$ and $A_3^{+3}B_5^{+3}O_{12}$ compounds have the perovskite and garnet structures respectively. It is noteworth that the oxides of the trivalent cations, $A_2^{+3}O_3$, may be considered in a general way as $A^{+3}B^{+3}O_3$ ($A^{+3}A^{+3}O_3$) type compounds. None of these $A_2^{+3}O_3$ oxides, however, are known to have a perovskite structure. Goldschmidt and his coworkers [2] were perhaps the first to investigate $A^{+3}B^{+3}O_3$ compounds in detail. Many other investigators, including Keith and Roy [3], Roth [4], and Geller and his coworkers [5, 6, 7] have substantially contributed to the data available on this formula-type compound.

The purpose of the present investigation was to survey the various structure types that occur under equilibrium conditions for different binary mixtures of the oxides of the trivalent cations and to establish the subsolidus phase equilibria relationships for various systems. Special emphasis was given to a classification of the structure types found for equimolar mixtures according to the ionic radii of the constituent cations.

2. Sample Preparation and Test Methods

With the exception of Cr_2O_3 and Fe_2O_3 which were reagent grade, the materials used in this investigation had a purity of about 99.9 percent. Specimens were prepared from either 0.5 or 1.0 gram batches of various binary combinations of different oxides. Calculated amounts of each end member, corrected for ignition loss, were weighed to the nearest milligram. Each batch was mixed, formed into a $\frac{3}{8}$ in.-diam pellet by pressing at 10,000 $lb/in.^2$ and fired at some relatively low temperature (at least 800 °C) for varying lengths of time. Most of the specimens were then ground, remixed, again pressed into pellets and fired at successively higher temperatures until equilibrium was obtained.

All specimens containing In_2O_3 or Cr_2O_3, were ground, mixed, and then sealed in platinum tubes for the higher temperature heat treatments. The duration and temperature of each heat treatment generally varied with the particular system under consideration. In general, the specimens were slow cooled at approximately 4 °C/min. However, a few of the mixtures were quenched from elevated temperatures.

All heatings were performed in an air atmosphere using a conventional muffle furnace for the low temperature heats and a program-controlled tube furnace or a manually operated quench furnace for the heat treatment between 1000 and 1650 °C. An induction furnace, having as the susceptor a small iridium crucible, was used for heat treatments above 1650 °C. Temperatures were controlled to at least ±10 °C.

Equilibrium was considered to have been attained when the X-ray patterns of a specimen showed no change with successive heat treatment of the speci-

[^1]: Figures in brackets indicatet he literature references at the end of this paper.

men or when the X-ray powder data was consistent with the results predicted from a previous set of experiments. All specimens were examined at room temperature by X-ray diffraction with a Geiger-counter diffractometer employing nickel-filtered copper radiation.

3. Results

The data obtained in this investigation are given in table 1. The table lists six groups of binary systems, each having either Al_2O_3, Ga_2O_3, Cr_2O_3, Fe_2O_3, Sc_2O_3, or In_2O_3 as one component. Each of these groups in turn is arranged according to decreasing cation size of the second component. Selected literature references are included for compositions not studied experimentally in the present work. No attempt was made to incorporate into the table any data pertaining solely to mixtures involving only oxides of the trivalent rare earth cations. These data were reported in a recent publication by Schneider and Roth [1]. The table was designed primarily to present sufficient data to estimate the subsolidus phase relationships of a majority of the listed binary systems.

Figure 1 gives a classification of the various structure types found for equimolar mixtures of the oxides of the trivalent cations. The coordinates of the figure are the radii of the A^{+3} and B^{+3} cations. For convenience the larger cation in any mixture is taken as the A^{+3} cation (ordinate) and the smaller as B^{+3} (abscissa). The radii of the different cations are indicated on the figure by open triangles.[2] The solid triangles on the diagonal line represent the

---

[2] Radii values are according to Ahrens [8] with the exception of Y^{+3}, In^{+3} and Sc^{+3} which were taken from Roth and Schneider [9]. The following radii values were used throughout this report: La^{+3}–1.14 A, Ce^{+3}–1.07 A, Pr^{+3}–1.06 A, Nd^{+3}–1.04 A, Sm^{+3}–1.00 A, Eu^{+3}–.98 A, Gd^{+3}–.97 A, Tb^{+3}–.93 A, Dy^{+3}–.92 A, Ho^{+3}–.91 A, Y^{+3}–~.91 A, Er^{+3}–.89 A, Tm^{+3}–.87 A, Yb^{+3}–.86 A, Lu^{+3}–.85 A, In^{+3}–.77 A, Sc^{+3}–.68 A, Fe^{+3}–.64 A, Cr^{+3}–.63 A, Ga^{+3}–.62 A, and Al^{+3}–.51 A.
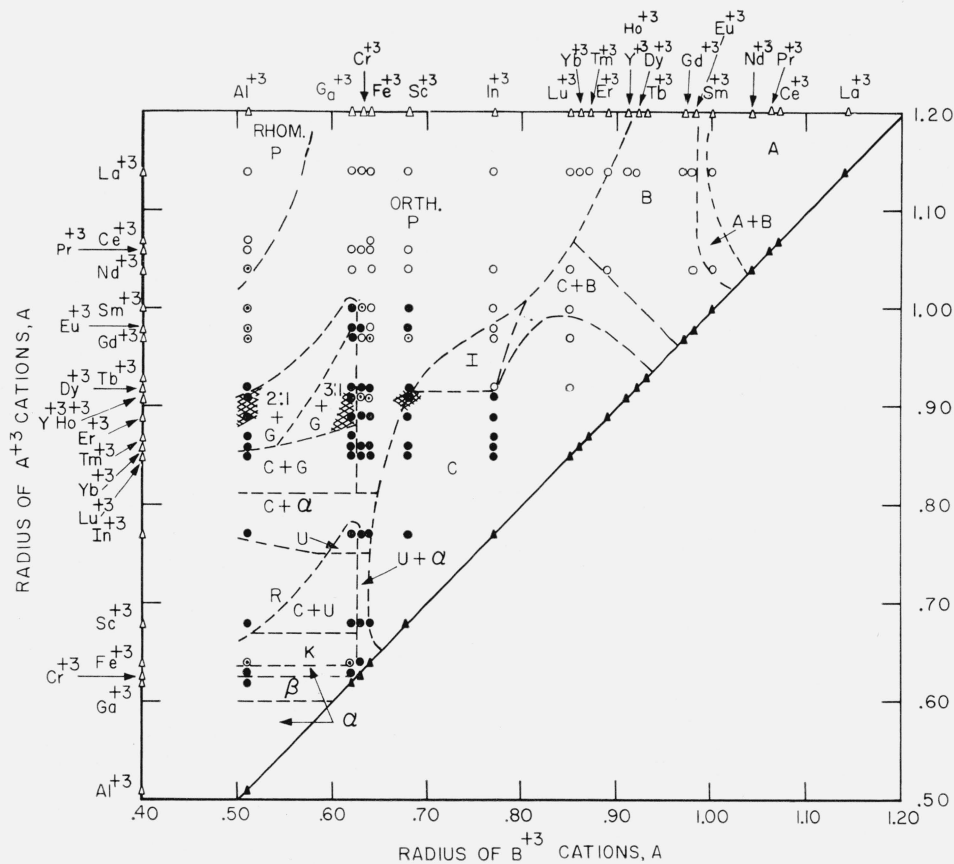
FIGURE 1. *Classification of structure types for equimolar mixtures of trivalent cations.*

△—radii of cations
▲—pure oxide
◐—compositions studied in present work
○—data taken from literature

A—A-type rare earth oxide
B—B-type rare earth oxide
C—C-type rare earth oxide
G—garnet
I—unknown type
α—corundum
β—beta gallia

K—kappa alumina
U—unknown type similar to kappa alumina
P—perovskite
R—unknown type
2:1—unknown type
3:1—unknown type

individual oxides. Each circle represents an equi-molar composition containing either one or two phases which have the indicated structures at room temperature. In most instances, these same types also exist stably at elevated temperatures. The one known exception to this is the listed structure of the 1:1 mixture of Fe_2O_3 and Al_2O_3 which is metastable at room temperature [10]. The diagram does not indicate any reversible phase transformations or decompositions that occur at elevated temperatures. It should be emphasized that the boundaries outlining each field were arbitrarily drawn. They do not indicate the division of different structure types for solid solutions which may exist between adjacent equimolar mixtures.

The occurrence of metastable phases was prevalent in a number of the double oxides which are near the boundary lines of figure 1. It was extremely difficult at times to establish the equilibrium phases. For this reason certain areas in the diagram are shaded to indicate that the position of certain portions of the boundary lines are somewhat in doubt. Several of these borderline systems are now being investigated in detail by the authors in order that the equilibrium phases can be definitely ascertained.

The majority of $A^{+3}B^{+3}O_3$ type compounds formed from double oxides of the trivalent cations are those having the perovskite structure. This field of perovskite types encompasses the largest single phase area of the diagram. The other single phase areas generally represent solid solutions and not true compounds. The two-phase areas, of course, contain compounds (3:1, 2:1, and 3:5) but not of the $A^{+3}B^{+3}O_3$ type.

Figure 1 not only designates the structure types for equimolar mixtures but also, with two exceptions, is applicable for all molar ratios of binary combinations of oxides of the listed cations. The two exceptions are the beta alumina (La_2O_3-Al_2O_3 and La_2O_3-Fe_2O_3 systems) and the spinel (Fe_2O_3-R_2O_3 systems) structures. The spinel structure, of course, occurs only when FeO is present as a third component. The various structure types are discussed in succeeding sections.

4. Discussion

4.1. A, B, C, Beta Gallia, and Corundum Structure Types

The structure type of the stable forms of the oxides of the trivalent cations (fig. 1, solid triangles) can be generally grouped in the following manner according to the ionic radius of the constituent cations: 1.14 A to 1.04 A-hexagonal A-type rare earth oxide structure; 1.00 A to 0.97 A-monoclinic B-type rare earth oxide structure; 0.93 A to 0.68 A-cubic C-type rare earth oxide structure; 0.64 A to 0.63A-rhombohedral corundum structure; 0.62 A-monoclinic beta gallia structure; and 0.51 A-rhombohedral corundum structure. In the above listing the structure types are seemingly out of order with respect to radii in that the beta gallia type is inter-mediate between two corundum types. This inconsistency emphasizes that other factors besides radii must be considered in generalizations such as given above.

Generally the effects of partial covalent bonding in essentially ionic type materials are neglected. Mooser and Pearson [11] related the structures of certain simple compounds to average quantum numbers and electronegativity values. From their work and others [11, 12] it is apparent that the covalent character (directional properties of the bonds) of a compound is directly related to the difference in the electronegativities of the cation and anion. Generally the greater the difference, the less the covalent type bonding. Using the electronegativity values given by Gordy and Thomas [13] to calculate relative covalent character, the aforementioned grouping of structure types can be rearranged according to increasing covalent character: A, B, or C types $(Ln_2O_3)^3$ < C-type (Sc_2O_3) < C-type (In_2O_3) < beta gallia type (Ga_2O_3) < corundum type (Al_2O_3) < corundum type (Cr_2O_3) < corundum type (Fe_2O_3). This method of arrangement, although on a very relative scale, does group like structure types together. It would be increasingly more difficult to apply this type of classification to compounds containing ions of different valence as well as those containing multiple ions of the same valence.

A number of the trivalent oxides have metastable polymorphs which have structures different from the stable modifications. A B-type structure has been reported for Nd_2O_3 [14], while Sm_2O_3, Eu_2O_3, and Gd_2O_3 are known to form the C-type [9]. Gallia (Ga_2O_3) and Al_2O_3 are similar in many respects in that they both have polymorphs of the same structure type. Gamma Al_2O_3 and gamma Ga_2O_3 are isostructural, as are alpha Al_2O_3 and alpha Ga_2O_3 [15]. This is also true for epsilon Ga_2O_3 and kappa Al_2O_3 and for beta Ga_2O_3 and theta Al_2O_3 [15]. A metastable polymorph of a pure oxide may appear as a stable phase in solid solutions. Examples of this occur in solid solutions between the oxides of the trivalent rare earth ions. For instance, the B-type structure in solid solutions is stable over a far greater range of average radii values than the pure oxides [1].

4.2. Perovskite Structure Type

The various combinations of double oxides that form 1:1 compounds which have the perovskite structure are indicated in figure 1. Each of these compounds has modifications which are distorted from the ideal cubic structure assuming either rhombohedral or orthorhombic symmetry at room temperature. At elevated temperatures other symmetries may occur. It has been suggested that the order of transformation with temperature is probably orthorhombic to rhombohedral to cubic [7].

Goldschmidt and coworkers [2] derived a tolerance factor (t) for the perovskite structure which is

---

[3] The symbol "Ln" represents the lanthanide series, lanthanum through lutecium.

given by the following formula:

$$t=\frac{R_A+R_O}{\sqrt{2}(R_B+R_O)}$$

where

$t=$tolerance factor
$R_A=$radius of larger cation
$R_B=$radius of smaller cation
$R_O=$radius of oxygen (1.40 A).

As t approaches unity, the tendency for the formation of a perovskite structure becomes greater. The lower limit or minimum value of t for a given series can only be determined experimentally. For the $Ln_2O_3 \cdot Ga_2O_3$ and $Ln_2O_3 \cdot Al_2O_3$ series of perovskite type compounds, the minimum values of t were found to be 0.85 and 0.84 respectively. In comparison, the lower limit of t for the other perovskite type series, $La_2O_3 \cdot Ln_2O_3$ [1], $Ln_2O_3 \cdot In_2O_3$, $Ln_2O_3 \cdot Sc_2O_3$, $Ln_2O_3 \cdot Fe_2O_3$ and $Ln_2O_3 \cdot Cr_2O_3$, are all equal to about 0.78.

Dalziel [16], considering only the Fe_2O_3, Ga_2O_3, and Al_2O_3 perovskite series, attempted to explain the differences in minimum t values on the basis of partial covalent character of the non rare earth cation-oxygen bond. To test the relative covalent character of the different series, Dalziel presented a graph similar to that given in figure 2. Expanding Dalziel's graph to include all appropriate data in table 1, figure 2 shows the relationship between the volumes of the Ln^{+3} cations in 12-fold coordination and the volumes of one formula weight of $Ln_2O_3 \cdot M_2O_3$ perovskite type compounds, as both determined experimentally (solid lines) and as predicted from the lanthanide contraction (dashed lines). For a given series, the volumes should decrease in a regular manner with the lanthanide contraction. The decrease, however, will be modified somewhat from that predicted, due to: (1) the deviation from close packing caused by increased distortion of the lattice and (2) the influence of covalent character of the cation-oxygen bonds [16]. The former would result in larger volumes than those predicted while the latter would produce an opposite effect.

In general, it can be concluded from figure 2 that for a given series, the covalent character significantly increases as the size of the Ln^{+3} cation decreases. It is difficult to compare the different series with regard to which group is more covalent because of
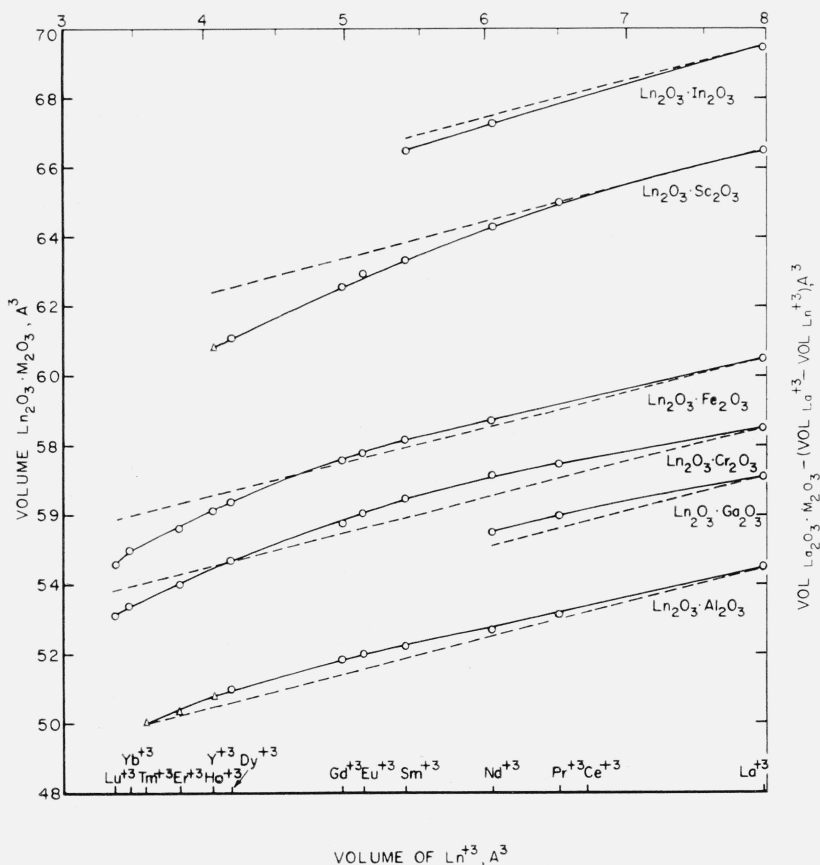

FIGURE 2. *Relationship between volumes of one formula weight of $Ln_2O_3 \cdot M_2O_3$ perovskites and volumes of cations in 12-fold coordination.*

Solid Curve—Determined experimentally
Dashed Curve—Predicted from lanthanide contraction, $[V_{La_2O_3 \cdot M_2O_3}-(V_{La}-V_{Ln})]$
⊙—Stable compound
△—Possibly metastable compound

masking effects of the various factors. It does appear, however, that the effect of partial covalent bonding is less pronounced in the Al_2O_3 and perhaps the Ga_2O_3 series than in the other groups. This would account for the larger minimum tolerance factors of the Al_2O_3 and Ga_2O_3 series.

4.3. Garnet Structure Type

The garnet structure occurs at the ideal 3:5 molar ratio in a number of binary systems involving oxides of the trivalent cations. Specifically, these include systems containing either Fe_2O_3, Ga_2O_3, or Al_2O_3 as one end member and a rare earth oxide (or Y_2O_3) as the other. The chemical formula of a garnet type compound can be written as $[A_3^{+3}][B_2^{+3}][C_3^{+3}]O_{12}$, where $[A^{+3}]$, $[B^{+3}]$, and $[C^{+3}]$ indicate cations which occur in 8-fold, 6-fold, and 4-fold coordination, respectively [17]. In binary systems the rare earth cations or Y^{+3} can be usually thought of as occupying the $[A^{+3}]$ sites with the smaller cations, Fe^{+3}, Ga^{+3}, or Al^{+3} filling the $[B^{+3}]$ and $[C^{+3}]$ positions.

Compounds having the garnet structure do not occur in binary systems containing Cr_2O_3. This agrees with the observation [17] that Cr^{+3} prefers only octahedral type of coordination ($[B^{+3}]$ sites) in the garnet structure. Apparently the Cr^{+3} cations will never appreciably occupy tetrahedral sites in the garnet structure, even when it is the most likely cation to be tetrahedrally coordinated.

Solid solution of the garnet type compounds which occurs in binary systems containing Ga_2O_3 has been generally overlooked because of the simultaneous report of solid solution between the perovskite and garnet structures in the Y_2O_3-Al_2O_3 system [3]. Solid solution definitely occurs in many binary gallia garnets. Figure 3 shows plots of the radii of the rare earth cations against both the compositional range of solid solution of the various garnet compounds (no. 1) and the corresponding change in unit cell dimensions (no. 2). In these garnet solid solutions, the rare earth cation apparently subsitutes for Ga^{+3} in the octahedral ($[B^{+3}]$) positions.[4]

The amount of solid solution as well as the amount of change in unit cell dimensions increases to a maximum at about Tm^{+3} as the size of the constituent rare earth cation decreases. The reason for this behavior is unknown. In addition, the values determined for the garnet solid solution in the Y_2O_3-Ga_2O_3 system were excessively larger than expected and do not fit the general curves of figure 3.

It is interesting to observe that solid solution of the garnet type compound for the gallia series occurs only in binary systems in which a perovskite-type compound does not exist as a stable phase. On this premise it was considered likely and experimentally verified that solid solution does occur in the smaller alumina garnets, $3Yb_2O_3 \cdot 5Al_2O_3$ and $3Lu_2O_3 \cdot 5Al_2O_3$. Although not determined exactly, the extent of garnet solid solution is fairly small, probably about
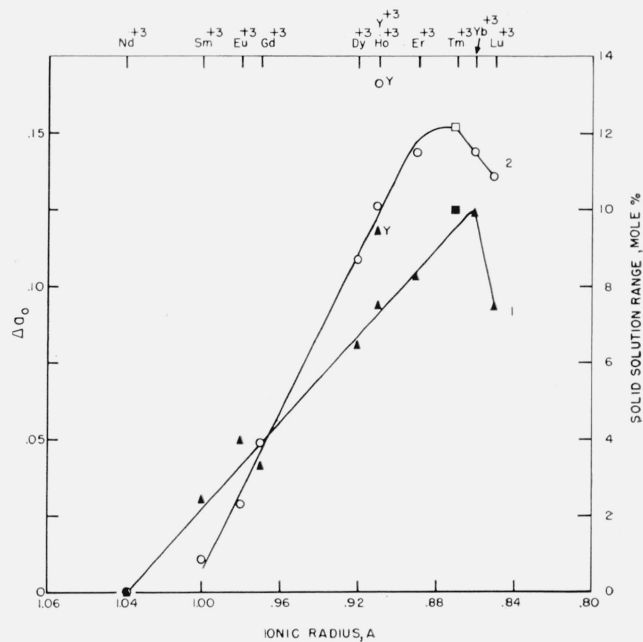
FIGURE 3. *Relationship between ionic radii and both compositional range of solid solution and corresponding parameter change in several gallia garnets at 1500 °C.*

Curve 1—Solid solution range
Curve 2—Change in unit cell dimension
$\triangle a_0 = a_0 \text{ 1:1} - a_0 \text{ 3:5}$
$\square$ = estimated

two mole percent. Substitutional type solid solution of the Fe_2O_3 garnets probably does not occur. However, as illustrated by the Y_2O_3-Fe_2O_3 system [18], partial reduction of Fe_2O_3 in these garnets may produce solid solution to a limited extent.

4.4. Kappa Alumina Structure Type

Considerable confusion exists in the literature with regard to the various low temperature, metastable polymorphs of Al_2O_3 and Ga_2O_3. These polytypes are ill-defined primarily because of the inability to obtain clear, interpretable X-ray diffraction data. Of particular interest in the present investigation are the kappa alumina and epsilon gallia polymorphs and their characteristic structures. Roy et al. [15] have clearly demonstrated through a series of solid solution studies that kappa alumina and epsilon gallia in reality have the same structure. The alumina polymorph having the kappa alumina structure has been reported [19] to be orthorhombic with $a = 8.49$ A, $b = 12.73$ A, and $c = 13.39$ A. The reported d-spacings were not given with sufficient accuracy to verify the cell dimensions.

Richardson et al. [20] described the phase which occurs at the equimolar mixture of Fe_2O_3 and Al_2O_3 as having a structure similar to that of kappa alumina. The X-ray pattern for the $50Fe_2O_3$: $50Al_2O_3$ phase was indexed by Richardson et al. [20] on the basis of an orthorhombic cell with $a = 7.03$ A, $b = 6.33$ A, and $c = 7.41$ A.[5] However, the calculated

---

[4] It has been suggested by S. Geller in a private communication that the solid solution may be of the interstitial and/or vacancy types instead of substitutional and thus result in a defect structure.

[5] Unit cell dimensions converted from kX units.

and observed *d*-spacings do not appear to be in close enough agreement to justify the reported indexing. In the present investigation three $Fe_2O_3-Al_2O_3$ mixtures, 47:53, 50:50, and 53:47 were prepared. Each specimen contained the same single phase as that reported by Richardson et al. [20]. The X-ray pattern of the $53Fe_2O_3:47Al_2O_3$ specimen was successfully indexed on the basis of an orthorhombic cell with $a=8.59$ A, $b=9.23$ A, and $c=4.98$ A as given in table 2. The indexing was accomplished only after comparison with the X-ray pattern of the $50Fe_2O_3:50Ga_2O_3$ specimen, a phase described by Wood [21]. The orthorhombic phases which occur in the $Fe_2O_3-Al_2O_3$ and $Fe_2O_3-Ga_2O_3$ systems are apparently isostructural and represent solid solutions rather than compounds. The similarity in structures is important because of the reported magnetic and piezoelectric properties of the $(1-x)Fe_2O_3 \cdot xGa_2O_3{}_{ss}$ phase. These properties in $(1-x)Fe_2O_3 \cdot xAl_2O_3{}_{ss}$ will be reported on in a future publication. Muan and Somiya [10] reported the complete phase relations for the $Fe_2O_3-Al_2O_3$ system and showed that the orthorhombic phase has both a minimum and maximum decomposition temperature.

There is not yet sufficient evidence to classify the orthorhombic phases of the $Fe_2O_3-Al_2O_3$ and $Fe_2O_3-Ga_2O_3$ systems as having a kappa alumina structure although there is a definite similarity. The X-ray patterns given in the literature for the kappa alumina and epsilon gallia polymorphs could not be indexed on the same basis as that given for $53Fe_2O_3:47Al_2O_3$ in table 2. The failure to index these patterns may be due to the inaccurate X-ray data available rather than dissimilar structures.

TABLE 2.   *X-ray powder diffraction data for* $(1-x)Fe_2O_3 \cdot xAl_2O_3{}_{ss}$

(53Fe₂O₃ : 47Al₂O₃ mixture)

hkl [1]	d [2]	I [3]	$\frac{1}{d^2}$ obs	$\frac{1}{d^2}$ cal
	A		A⁻²	A⁻²
100	6.03	25	0.0253	0.0253
020	4.64	23	.0464	.0470
111	3.90	18	.0657	.0656
121	} 3.144	38	.1012	{ .1008
220				.1012
130	2.899	38	.1190	.1193
221	2.658	100	.1415	.1415
131	} 2.497	29	.1604	{ .1596
002				.1610
012	2.407	18	.1726	.1728
102	} 2.393	34	.1747	{ .1746
311				.1741
040	2.306	14	.1881	.1881
022	2.193	23	.2080	.2080
321	2.186	38	.2093	.2093
400	2.146	13	.2171	.2171
122	2.125	21	.2214	.2216
331	1.9000	29	.2679	.2681
042	1.6920	20	.3493	.3491
123	1.5377	16	.4226	.4229

[1] Based on orthorhombic cell with $a=8.59$ A, $b=9.23$ A, and $c=4.98$ A.
[2] Interplanar spacing.
[3] Relative intensity.

Figure 4, as well as table 3, presents X-ray powder data for all the phases encountered in this investigation which may have structures similar to kappa alumina. It is apparent, from figure 4, that the patterns for kappa alumina, epsilon gallia, $50Fe_2O_3:50Al_2O_3$ and $50Fe_2O_3:50Ga_2O_3$ are related. Each of the X-ray patterns of the other phases, $50In_2O_3:$
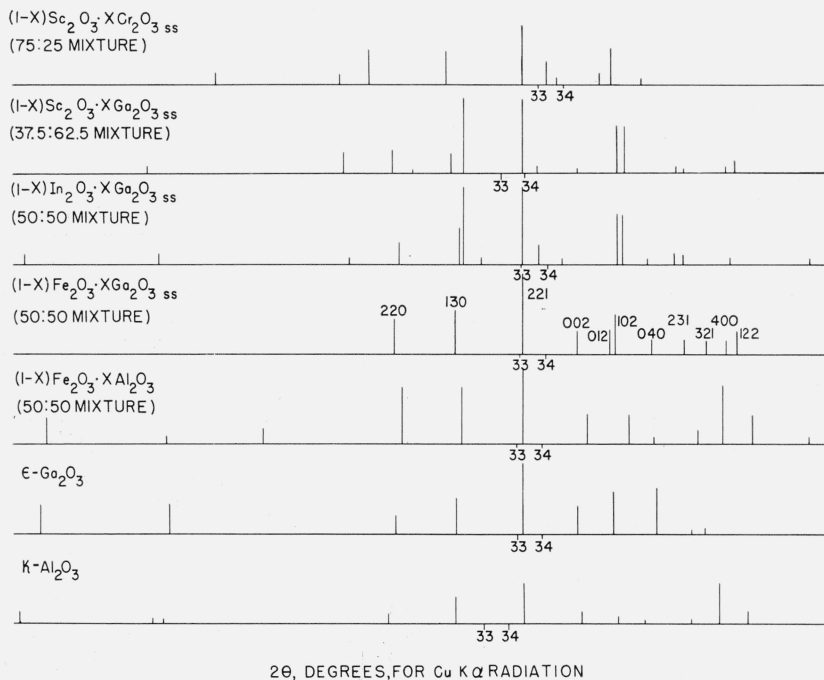
FIGURE 4.   *Diagrammatic X-ray powder diffraction patterns for kappa alumina [25], epsilon gallia [15], 50Fe₂O₃:50Al₂O₃ 50Fe₂O₃:50Ga₂O₃, 50In₂O₃:50Ga₂O₃, 37.5Sc₂O₃:62.5Ga₂O₃ and 75Sc₂O₃:25Cr₂O₃.*

For the kappa alumina pattern, d-values apparently due to extraneous phases were deleted, as was done by Roy et al. [15].

TABLE 3. *X-ray powder diffraction data for* $(1-x)\mathrm{In_2O_3}\cdot x\mathrm{Ga_2O_3}$ $_{ss}$, $(1-x)\mathrm{Sc_2O_3}\cdot x\mathrm{Ga_2O_3}$ $_{ss}$, *and* $(1-x)\mathrm{Sc_2O_3}\cdot x\mathrm{Cr_2O_3}$ $_{ss}$

50In₂O₃:50Ga₂O₃ mixture		37.5Sc₂O₃:62.5Ga₂O₃ mixture		75Sc₂O₃:25Cr₂O₃ mixture	
d^1	I^2	d^1	I^2	d^1	I^2
A		A		A	
9.72	13	4.73	12	4.44	18
6.83	18	3.404	36	3.559	21
4.88	9	3.110	39	3.400	59
4.84	17	3.034	8	3.046	57
3.423	11	2.889	29	2.763	100
3.183	37	2.878	100	2.687	45
2.279	57	2.852	100	2.653	12
2.917	100	2.653	88	2.531	15
2.851	11	2.598	16	2.501	52
2.710	100	2.486	11	2.417	9
2.661	57	2.385	88	1.9713	13
2.590	9	2.365	90	1.9465	49
2.437	80	2.247	13	1.9072	80
2.426	80	2.231	8	1.7984	11
2.363	11	2.144	14	1.7172	16
2.298	15	2.131	24	1.6573	49
2.279	8	1.830	6	1.6247	15
2.177	13	1.7905	52	1.6861	27
2.031	13	1.7836	39	1.4903	11
1.9434	8	1.7077	46	1.4666	15
1.9155	9	1.6800	100	1.4395	10
1.8273	33	1.6017	52	1.4221	10
1.8200	34	1.5858	10	1.4127	10
1.7190	100	1.5793	28	1.3902	10
1.6709	8			1.3824	10
1.6345	25	1.5167	24	1.3442	10
1.6148	23			1.3180	11
1.6055	8	1.4933	10	1.2514	11
1.5494	31	1.4890	10		
1.5253	11	1.4839	49		
		1.4447	54		
1.5217	11	1.4328	11		
1.5176	24				
1.5158	32				
1.4784	26	1.4281	24		
1.4756	39	1.4158	42		
		1.3966	48		
1.4592	14	1.3640	9		
1.4551	15				
1.4491	30	1.3496	11		
1.4265	42				
1.3937	14	1.3466	11		
		1.3267	13		
1.3816	9	1.3048	18		
1.3558	14				
1.3310	8				

[1] Interplanar spacing.
[2] Relative intensity.

TABLE 4. *X-ray powder diffraction data for* $(1-x)\mathrm{Sc_2O_3}\cdot x\mathrm{Al_2O_3}$ $_{ss}$

(50Sc₂O₃: 50Al₂O₃ mixture)

Rhom. hkl [1]	d [2]	I [3]	$\frac{1}{d^2}$obs	$\frac{1}{d^2}$cal
	A		A⁻²	A⁻²
222	2.842	29	0.1238	0.1238
2̄2̄2̄	2.687	100	.1385	.1385
040	2.359	21	.1797	.1798
04̄1/23̄2	2.265	5	.1940	.1948
22̄3̄	2.241	5	.1991	.1984
240	2.138	7	.2185	.2174
332	2.004	9	.2491	.2500
04̄3	1.8496	5	.2923	.2920
15̄2̄	1.7051	21	.3440	.3436
044̄	1.6350	28	.3741	.3741
26̄2̄	1.4180	12	.4973	.4979
2̄6̄2̄	1.3990	5	.5123	.5130

[1] Rhombohedral cell, $a=9.45$ A, $\alpha=87.4°$.
Hexagonal cell, $a=13.07$ A, $c=17.05$ A.
[2] Interplanar spacing.
[3] Relative intensity.

50Ga₂O₃, 37.5Sc₂O₃:62.5Ga₂O₃, and 75Sc₂O₃:25Cr₂O₃, could not be indexed although they, too, appear similar to the pattern of kappa alumina. It would seem, strictly by the comparison of X-ray patterns, that In₂O₃-Ga₂O₃ and Sc₂O₃-Ga₂O₃ phases are isostructural with each other, but not necessarily with kappa alumina. The phase most dissimilar with kappa alumina in this entire group is that of 75Sc₂O₃:25Cr₂O₃.

4.5. Other Structure Types

Keith and Roy [3] reported that an unknown phase occurs in a melted 50:50 mixture of In₂O₃ and Al₂O₃. They designated this phase as a high form of In₂O₃: Al₂O₃ and listed several of its X-ray reflections. In an effort to obtain this phase, the experiment of Keith and Roy was repeated. The melted specimen of 50:50 In₂O₃-Al₂O₃ contained two phases, In₂O₃ and apparently the same phase as reported by Keith and Roy. Other experiments with the 50In₂O₃: 50Al₂O₃ mixture indicated that the unknown phase is probably metastable in the In₂O₃-Al₂O₃ system and occurs only on quenching the melt.

In the Sc₂O₃-Al₂O₃ system a stable phase occurs which, according to X-ray powder data, appears to be isostructural with the metastable phase of the In₂O₃-Al₂O₃ system. This phase occurs over a region of Sc₂O₃-Al₂O₃ compositions and represents a solid solution and not a true compound. The X-ray pattern of the 50Sc₂O₃:50Al₂O₃ mixture is given in table 4. The pattern was indexed on the basis of a rhombohedral cell by comparison with the pattern of 2PbO·Nb₂O₅, a rhombohedral distortion of the pyrochlore structure. The X-ray pattern for the Sc₂O₃-Al₂O₃ phase was diffuse regardless of heat treatment of the specimen, and therefore the agreement between observed and calculated values, given in table 4, is only fair for the less intense reflections. Single crystal data is needed to ascertain the correct structure type. Superstructure peaks, necessary to differentiate a body centered C-type structure or a face centered pyrochlore structure from the fluorite or Sb₂O₃-type structures, could not be found in the X-ray pattern. The fluorite structure would require that all the oxygen vacancies be disordered. For the Sc₂O₃-Al₂O₃ phase to have a C-type or a Sb₂O₃-type structure a complete ordering of the vacant oxygen sites would be required while the pyrochlore structure would necessitate only partial ordering.

A number of different phases encountered in this investigation have not been identified or even related with a specific known structure type. These phases, apparently all compounds, exist in various systems at either the 3:1, 2:1 or 1:1 molar compositions. The 3:1 compounds occur exclusively in galliate systems; specifically, Ga₂O₃ with either Sm₂O₃, Eu₂O₃, Gd₂O₃, Dy₂O₃, Ho₂O₃, Y₂O₃, or Er₂O₃. These compounds, all apparently isostructural, have not been previously reported. The X-ray data of 3Gd₂O₃· Ga₂O₃, which is given in table 5, is typical of all the patterns of these isostructural 3:1 compounds. The only

difference between the various patterns is the appropriate shift in the d-spacings of the X-ray reflections due to cation size differences. It is noteworthy that the 3:1 compound does not occur in systems in which a perovskite type compound forms as a stable phase.

A series of apparently isostructural 2:1 compounds exist in both aluminate and galliate systems. The first 2:1 compound of this type studied extensively was the $2Y_2O_3 \cdot Al_2O_3$ phase [22]. In binary aluminate systems, Gd^{+3}, Dy^{+3}, Ho^{+3}, Er^{+3}, Tm^{+3}, and Yb^{+3} can be substituted for Y^{+3}. In galliate systems, however, only the oxides of the larger cations La^{+3}, Nd^{+3}, Sm^{+3}, and Eu^{+3} form 2:1 compounds with Ga_2O_3. Evidently this structure type is dependent on radius ratios and will only occur within specific ranges of cation radii values. An example of this occurs in the Yb_2O_3-Al_2O_3 and Lu_2O_3-Al_2O_3 systems. The 2:1 compound forms in the Yb_2O_3-Al_2O_3 system but not in the Lu_2O_3-Al_2O_3 system, even though the radius of Lu^{+3} is only 0.01 A smaller than that of Yb^{+3}. However, the X-ray pattern of the 3:5 mixture in the Lu_2O_3-Al_2O_3 system showed, in addition to the garnet peaks, a few minor reflections which may represent a 2:1 phase. At present, it would appear that the occurrence of a 2:1 compound in the Lu_2O_3-Al_2O_3 system is strictly a metastable phenomenon.

Table 6 compares the X-ray pattern for $2Y_2O_3 \cdot Al_2O_3$ obtained in this investigation with that reported by Warshaw and Roy [22]. They described this 2:1 phase as being distorted cubic with a primitive lattice. Because of certain line splitting in the X-ray pattern, they infer that the material may actually have rhombohedral symmetry. The two patterns given in table 6 are very similar and obviously represent the same phase; neither pattern could be indexed in the present work. It is evident, from the present X-ray data, that $2Y_2O_3 \cdot Al_2O_3$ has low symmetry and cannot be designated as cubic or rhombohedral.

The only $A^{+3}B^{+3}O_3$ type compounds found in the present investigation which do not have the perovskite structure are those which occur in the Eu_2O_3-In_2O_3, Gd_2O_3-In_2O_3, and Dy_2O_3-In_2O_3 systems (designated as I in fig. 1). These 1:1 compounds will be reported on more extensively in a following publication [23]. The $Eu_2O_3 \cdot In_2O_3$, $Gd_2O_3 \cdot In_2O_3$, and $Dy_2O_3 \cdot In_2O_3$ compounds appear to be isostructural, having pseudohexagonal symmetry. The $Dy_2O_3 \cdot In_2O_3$ compound apparently decomposes between 1600 °C and 1650 °C to a mixture of B- and C-rare earth oxide structure types.

4.6. Subsolidus Phase Equilibria Relationships

Figure 5 gives the subsolidus phase equilibria relationships for various binary combinations of oxides of the trivalent cations. The figure is divided into

TABLE 5. *X-ray powder diffraction data for* 3 $Gd_2O_3 \cdot Ga_2O$

d [1]	I [2]	d [1]	I [2]
4.53	20	2.005	30
4.11	13	1.9918	15
3.204	14		
3.054	100	1.9027	15
3.025	57	1.8349	32
		1.8097	14
2.990	27	1.7672	17
2.908	22	1.7184	17
2.824	29		
2.630	17	1.6808	17
2.301	15	1.6450	24
		1.5788	24
2.241	17	1.5456	17
2.199	13	1.5276	25
2.032	39		

[1] Interplanar spacing.
[2] Relative intensity.

TABLE 6. *X-ray powder diffraction data for* $2Y_2O_3 \cdot Al_2O_3$

hkl	Warshaw and Roy [22]		Present work		hkl [1]	Warshaw and Roy [22]		Present work	
	d [2]	I [3]	d [2]	I [3]		d [2]	I [3]	d [2]	I [3]
110	7.46	10	7.41	63				1.9811	16
200	5.28	3	5.26	16				1.9449	15
210	4.71	22	4.69	100				1.9163	12
			4.54	16				1.9027	16
220	3.71	7	3.705	19	440	1.843	18	1.8426	80
310	3.33	33	3.326	100	522/441 [4]	1.828	20	1.8298	85
301	3.01	100	3.011	100+	522/441 [4]	1.816	19	1.8164	81
320	2.91	94	2.908	100	530/433	1.793	7	1.7921	32
			2.884	47	600/442	1.732	10	1.7317	32
400	2.62	17	2.615	48	610 [4]	1.722	13	1.7235	61
410/322 [4]	2.56	10	2.559	64	610 [4]	1.716	13		
410/322 [4]	2.53	10	2.538	29	611/532	1.711	8		
			2.523	61				1.6279	27
			2.486	21				1.6236	20
			2.470	39				1.6126	23
330/411	2.46	9	2.454	37	622	1.575	9	1.5759	41
421 [4]	2.29	7	2.291	43				1.5661	45
421 [4]	2.27	7	2.274	28	630/542	1.561	12	1.5621	60
			2.129	12	631	1.551	7	1.5504	44
500/430	2.07	22	2.090	13				1.5065	32
510/431	2.06	12	2.063	87	543/710/550	1.484	4	1.4847	27
			2.046	41				1.4809	24
								1.4541	15
					720/641	1.436	4	1.4379	23
								1.3850	15

[1] Based on cubic cell with $a = 10.40$ A [22].
[2] Interplanar spacing.
[3] Relative intensity.
[4] "Splitting may represent a possible rhombohedral distortion of the cubic lattice" [22].

six groups of diagrams, each having either Al_2O_3, Ga_2O_3, Cr_2O_3, Fe_2O_3, Sc_2O_3, or In_2O_3 as one component. Previously published diagrams pertinent to a given series are not reproduced here but are included as literature references in the legend of the figure.

All the diagrams were drawn primarily from the data contained in table 1. Data points are indicated by circles on the diagrams. In some instances entire diagrams, or portions thereof, were estimated from the phase relations of similar known systems. The boundaries of the garnet solid solutions were determined by the parametric method while the solid solution areas of A-, B-, or C-type phases were established by a variation of this method as previously described [1]. The boundaries of most of the other type solid solution areas were approximated from X-ray patterns on the basis of the relative amounts of each phase present in a specimen containing two phases. Possible variations of solid solubility with temperature have been ignored in this work. In general, the diagrams must be considered as approximate and minor shifts in solid solution boundary limits may be expected.

The subsolidus phase diagram for the Y_2O_3-Al_2O_3 system has been included in figure 5a although the diagram has been previously published by Warshaw and Roy [22]. The present diagram differs from the previous one in that a 1:1 perovskite type compound is shown to have a region of stability at elevated temperatures. At lower temperatures, the compound apparently decomposes to a mixture of $2Y_2O_3 \cdot Al_2O_3$ and $3Y_2O_3 \cdot 5Al_2O_3$. The present work does not contradict the published data, but merely extends to temperature ranges not previously reported. A complete reinvestigation of this system is now being undertaken. Because the stability of the 1:1 compound in the Y_2O_3-Al_2O_3 system is still unknown, the stability of the perovskite phase in the related systems of Ho_2O_3-Al_2O_3 and Er_2O_3-Al_2O_3 is also in doubt.

Perhaps one of the more interesting systems investigated is that of Dy_2O_3-In_2O_3, figure 5f. The phase diagram of this system indicates a solid solution area of B-type rare earth oxide. Since Dy_2O_3 and In_2O_3 both have the C-type structure, it is unusual for a B-type structure to occur. The largest average cation radius of the B-type solid solution in the Dy_2O_3-In_2O_3 system is about 0.87 A. This value is appreciably smaller than the radius of Gd^{+3} (0.97 A) which is the smallest rare earth ion to form a pure B-type oxide. Goldschmidt et al. [24] reported that Dy_2O_3 formed a B-type structure at elevated temperatures but his work has not yet been confirmed [9]. The formation of the solid solution area of B-type in the Dy_2O_3-In_2O_3 system might actually indicate that Dy_2O_3 does transform from C- to B-type in the pure state. Specimens of Dy_2O_3 heated above the melting point of platinum shattered in a manner indicative of a possible reversible phase transformation.

5. Summary

A survey was made of the subsolidus reactions that occur in various binary systems involving oxides of the trivalent cations. Incorporated into the study were Al_2O_3, Ga_2O_3, Cr_2O_3, Fe_2O_3, Sc_2O_3, In_2O_3, Y_2O_3, and most of the trivalent rare earth oxides. Mixtures in 69 different binary systems were investigated. Specimens were heated at various temperatures until equilibrium was attained and then examined at room temperature by X-ray powder diffraction techniques.

According to the radii of constituent cations, a classification was made of the structure types of the various phases found for equimolar mixtures. The classification consists of a plot of the radii of A^{+3} cations versus the radii of B^{+3} cations and shows specific regions of stability for the different structure types. The graph is divided into regions of one and two phase areas and represents, in addition to several unknown types, the following structures: A-, B-, and C-type rare earth oxide; corundum; beta gallia; kappa alumina; garnet; and perovskite. The classification essentially summarizes the structure types found in all possible binary mixtures of oxides of the trivalent cations studied.

With one exception, all the $A^{+3}B^{+3}O_3$ type compounds which occur have the perovskite structure. The minimum tolerance factors of the alumina and gallia series of perovskite compounds are significantly larger than the Cr_2O_3, Fe_2O_3, Sc_2O_3, and In_2O_3 series. The appreciable difference in minimum tolerance factor apparently can be related to the effect of partial covalent bonding.

Appreciable solid solution of the garnet type compounds occurs in binary systems containing Ga_2O_3. The range of solid solution generally increases to a maximum at about Tm^{+3} as the radii of the rare earth cation decreases. Solid solution of the garnet compound does not occur in binary systems containing a stable perovskite phase.

Based on the similarity of X-ray patterns, the structure of kappa alumina appears to be related to the structures of $(1-x)Fe_2O_3 \cdot xAl_2O_3$ ss and $(1-x)Fe_2O_3 \cdot xGa_2O_3$ ss. There is also a similarity between these phases and other solid solution phases which occur in the In_2O_3-Ga_2O_3, Sc_2O_3-Ga_2O_3, and Sc_2O_3-Cr_2O_3 systems.

A 2:1 compound occurs in a number of those systems containing either Al_2O_3 or Ga_2O_3 as one component. A 3:1 compound occurs exclusively in systems containing Ga_2O_3. The structures of the 2:1 and 3:1 compounds were not related to any known structure type. A rhombohedral phase which occurs stably in the Sc_2O_3-Al_2O_3 system and metastably in the In_2O_3-Al_2O_3 system may have either a fluorite, Sb_2O_3, pyrochlore, or C-type structure.

The subsolidus phase assemblages for 79 binary systems were predicted from the data compiled in this investigation.

TABLE 1.—*Binary oxide mixtures of the trivalent cations*

Al[+3] and larger cations

System	Composition	Heat [1] treatment		Phases identified by X-ray diffraction	Structure type	Symmetry	Unit cell dimensions				Remarks	References [2]
		Temp.	Time				a	b	c	α		
	Mole %	°C	hr				A	A	A	deg		
La$_2$O$_3$–Al$_2$O$_3$	50:50	------	------	La$_2$O$_3$·Al$_2$O$_3$	Perovskite	Rhombohedral	5.357			60.1	Rhombohedral to cubic transformation occurs at 435±25 °C [7].	Geller and Bala [7].
	8.3:91.7	1800	1	La$_2$O$_3$·11Al$_2$O$_3$	Beta alumina	Hexagonal	5.556		22.030			Roth and Hasko [31].
Ce$_2$O$_3$–Al$_2$O$_3$	50:50	1600	1	Ce$_2$O$_3$·Al$_2$O$_3$	Perovskite	Rhombohedral	3.766			90.2	Unit cell dimensions based on face-centered pseudo cell.	Roth [4].
Pr$_2$O$_3$–Al$_2$O$_3$	50:50	------	------	Pr$_2$O$_3$·Al$_2$O$_3$	Perovskite	Rhombohedral	5.307			60.33		Geller and Bala [7].
Nd$_2$O$_3$–Al$_2$O$_3$	66.7:33.3	1350	6									
		1500	6									
		1650	6	Nd$_2$O$_3$+Nd$_2$O$_3$·Al$_2$O$_3$	A-type + perovskite	Hexagonal+rhombohedral.						
	50:50	------	------	Nd$_2$O$_3$·Al$_2$O$_3$	Perovskite	Rhombohedral	5.286			60.42		Geller and Bala [7].
	37.5:62.5	1350	6									
		1500	6									
		1650	6	Nd$_2$O$_3$·Al$_2$O$_3$	Perovskite	Rhombohedral					Al$_2$O$_3$ not detected; equilibrium phases probably Nd$_2$O$_3$·Al$_2$O$_3$+Al$_2$O$_3$.	
Sm$_2$O$_3$–Al$_2$O$_3$	66.7:33.3	1350	6									
		1500	6									
		1650	6	Sm$_2$O$_3$+Sm$_2$O$_3$·Al$_2$O$_3$	B-type+perovskite	Monoclinic+orthorhombic.						
	50:50	------	------	Sm$_2$O$_3$·Al$_2$O$_3$	Perovskite	Orthorhombic.	5.285	5.290	7.473		Results confirmed in present work for specimen heat treated at 1650 °C. Orthorhombic to rhombohedral transformation occurs at 800 °C [6].	Geller and Bala [7]. Geller [6].
	37.5:62.5	1350	6									
		1650	6	Sm$_2$O$_3$·Al$_2$O$_3$	Perovskite	Orthorhombic					Al$_2$O$_3$ not detected; equilibrium phases probably Sm$_2$O$_3$·Al$_2$O$_3$+Al$_2$O$_3$.	
Eu$_2$O$_3$–Al$_2$O$_3$	50:50	------	------	Eu$_2$O$_3$·Al$_2$O$_3$	Perovskite	Orthorhombic	5.271	5.292	7.458		Results confirmed in present work for specimen heat treated at 1650 °C.	Geller and Bala [7].
Gd$_2$O$_3$–Al$_2$O$_3$	66.7:33.3			2Gd$_2$O$_3$·Al$_2$O$_3$	Unknown	Unknown					The 2:1 phase also forms in the following systems: Dy$_2$O$_3$–Al$_2$O$_3$, Ho$_2$O$_3$–Al$_2$O$_3$, Y$_2$O$_3$–Al$_2$O$_3$, Er$_2$O$_3$–Al$_2$O$_3$, Tm$_2$O$_3$–Al$_2$O$_3$ and Yb$_2$O$_3$–Al$_2$O$_3$ [32].	Warshaw and Roy [32].
	50:50	------	------	Gd$_2$O$_3$·Al$_2$O$_3$	Perovskite	Orthorhombic	5.247	5.304	7.417		Results confirmed in present work for specimen heat treated at 1650 °C.	Geller and Bala [7].
	37.5:62.5	1350	6									
		1650	6	Gd$_2$O$_3$·Al$_2$O$_3$+Al$_2$O$_3$	Perovskite+corundum.	Orthorhombic+rhombohedral.						
Dy$_2$O$_3$–Al$_2$O$_3$	50:50	1350	6									
		1650	6	Dy$_2$O$_3$·Al$_2$O$_3$+3Dy$_2$O$_3$·5Al$_2$O$_3$	Perovskite+garnet	Orthorhombic+cubic.					Nonequilibrium	
		1850	.17	Dy$_2$O$_3$·Al$_2$O$_3$	Perovskite	Orthorhombic	5.21	7.38	5.31			
	37.5:62.5	------	------	3Dy$_2$O$_3$·5Al$_2$O$_3$	Garnet	Cubic					Garnet phase (3:5) also forms in the following systems: Tb$_2$O$_3$–Al$_2$O$_3$, Ho$_2$O$_3$–Al$_2$O$_3$, Y$_2$O$_3$–Al$_2$O$_3$, Er$_2$O$_3$–Al$_2$O$_3$, Tm$_2$O$_3$–Al$_2$O$_3$, Yb$_2$O$_3$–Al$_2$O$_3$ and Lu$_2$O$_3$–Al$_2$O$_3$ [32].	Warshaw and Roy [32].
Ho$_2$O$_3$–Al$_2$O$_3$	50:50	1350	6									
		1650	6	2Ho$_2$O$_3$·Al$_2$O$_3$+Ho$_2$O$_3$·Al$_2$O$_3$+3Ho$_2$O$_3$·5Al$_2$O$_3$	Unknown+perovskite+garnet.	Unknown+orthorhombic++cubic.					Nonequilibrium	
		1850	.17	...do...	...do...	...do...					Nonequilibrium; 2Ho$_2$O$_3$·Al$_2$O$_3$ and 3Ho$_2$O$_3$·5Al$_2$O$_3$ decreased in amounts relative to previous heat.	
		1910	.5	Ho$_2$O$_3$·Al$_2$O$_3$	Perovskite	Orthorhombic	5.18	7.36	5.33			

System	Composition	Temp	Time	Compound								Remarks	Reference
Y_2O_3–Al_2O_3 [3a]	66.7:33.3	1100	16										Geller and Bala [7].
		1650	6	$2Y_2O_3 \cdot Al_2O_3$	Unknown	Unknown							
	50:50	------	------	$Y_2O_3 \cdot Al_2O_3$	Perovskite	Orthorhombic	5.179	5.329	7.370				
		1350	6										
		1500	6	$Y_2O_3 + 2Y_2O_3 \cdot Al_2O_3 + 3Y_2O_3 \cdot 5Al_2O_3 + Y_2O_3 \cdot Al_2O_3$	C-type+unknown+ garnet+perovskite.	Cubic+unknown+ cubic+orthorhombic.						Nonequilibrium	
		1850	.5	$Y_2O_3 \cdot Al_2O_3$	Perovskite	Orthorhombic						Perovskite apparently decomposing; nonequilibrium.	
		1705	.5	$Y_2O_3 \cdot Al_2O_3 + 2Y_2O_3 \cdot Al_2O_3 + 3Y_2O_3 \cdot 5Al_2O_3$	Perovskite+ unknown+garnet.	Orthorhombic+un- known+cubic.							
		1645	1	-----do-----	----do----	----do----						Garnet and 2:1 phases increased in amount relative to previous heat; nonequilibrium.	
	37.5:62.5	1650	2	$3Y_2O_3 \cdot 5Al_2O_3$	Garnet	Cubic	12.01						Yoder and Keith 33].
		1730	1	-----do-----	----do----	----do----						
Er_2O_3–Al_2O_3	75:25	1350	6										
		1500	6										
		1650	6	$Er_2O_3 + 2Er_2O_3 \cdot Al_2O_3$	C-type+unknown	Cubic+unknown							
	50:50	1350	6										
		1650	6	$Er_2O_3 + 2Er_2O_3 \cdot Al_2O_3 + Er_2O_3 \cdot Al_2O_3 + 3Er_2O_3 \cdot 5Al_2O_3$.	C−type+unknown+ perovskite+garnet.	Cubic+unknown +orthorhombic +cubic.	11.983					Nonequilibrium; listed dimension for garnet phase in mixture.	
		1800	.5	-----do-----	----do----	----do----						Nonequilibrium; no apparent change in relative amounts from previous heat.	
		1350	6										
		1650	6										
		1850	6	-----do-----	----do----	----do----						Nonequilibrium; C-type, 2:1 and garnet phases reduced in amount relative to 1650 °C heat.	
		1350	6										
		1650	6										
		1900	.75	$Er_2O_3 \cdot Al_2O_3$	Perovskite	Orthorhombic						Specimen melted	
		1350	6										
		1650	6										
		1910	.08										
		1840	.75	$Er_2O_3 \cdot Al_2O_3$	Perovskite	Orthorhombic	5.16	7.33	5.32			Specimen melted; then annealed	
	37.5:62.5	1350	6										
		1600	6										
		1650	12	$Er_2O_3 \cdot Al_2O_3 + 3Er_2O_3 \cdot 5Al_2O_3$	Perovskite+garnet	Orthorhombic+cubic	11.983					Nonequilibrium; listed dimension for garnet phase in mixture.	
Tm_2O_3–Al_2O_3	50:50	1350	6										
		1650	6	$2Tm_2O_3 \cdot Al_2O_3 + Tm_2O_3 \cdot Al_2O_3 + 3Tm_2O_3 \cdot 5Al_2O_3$.	Unknown+perovskite +garnet.	Unknown+ orthorhombic +cubic.	5.15 11.96	7.29	5.33			Nonequilibrium; listed dimensions for perovskite and garnet phases in mixture.	
		1850	.7	-----do-----	----do----	----do----						Nonequilibrium; no apparent change in relative amounts from previous heats.	
		1350	6										
		1650	6										
		1870	.08										
		1845	.25	$2Tm_2O_3 \cdot Al_2O_3 + Tm_2O_3 \cdot Al_2O_3 + 3Tm_2O_3 \cdot 5Al_2O_3$.	Unknown +perovskite +garnet.	Unknown +orthorhombic +cubic.						Specimen melted; then annealed. Nonequilibrium; perovskite consider- ably reduced in amount compared to 1850 °C specimen.	
	37.5:62.5	1350	6										
		1600	6										
		1650	12	$3Tm_2O_3 \cdot 5Al_2O_3$	garnet	Cubic	11.96						
Yb_2O_3–Al_2O_3	50:50	1350	6										
		1650	6	$Yb_2O_3 + 2Yb_2O_3 \cdot Al_2O_3 + 3Yb_2O_3 \cdot 5Al_2O_3$ ss.	C-type+unknown+ garnet.	Cubic+unknown+ cubic.	11.946					Nonequilibrium; listed dimension for garnet phase in mixture.	
		1770	0.33	-----do-----	----do----	----do----						Nonequilibrium C-type phase reduced in amount relative to previous heat.	
		1850	.33	-----do-----	----do----	----do----						Nonequilibrium; C-type phase reduced in amount relative to previous heat.	
	37.5:62.5	1350	6										
		1600	6										
		1650	12	$3Yb_2O_3 \cdot 5Al_2O_3$	Garnet	Cubic	11.931						
Lu_2O_3–Al_2O_3	50:50	1350	6										
		1650	6	$Lu_2O_3 + 3Lu_2O_3 \cdot 5Al_2O_3$ ss.	C-type+garnet	Cubic+cubic	11.927					Listed dimension for garnet phase in mixture.	
		1800	0.17	-----do-----	----do----								

See footnotes at end of table.

TABLE 1.—*Binary oxide mixtures of the trivalent cations*—Continued

Al^{+3} and larger cations—Continued

System	Composition	Heat[1] treatment Temp.	Time	Phases identified by X-ray diffraction	Structure type	Symmetry	Unit cell dimensions a	b	c	α	Remarks	References[2]
	Mole %	°C	hr				A	A	A	deg		
	37.5:62.7	1350	6									
		1600	6									
		1650	6	3Lu$_2$O$_3$·5Al$_2$O$_3$	Garnet	Cubic	11.912				May be some 2:1 phase present	
In$_2$O$_3$–Al$_2$O$_3$	50:50	800	20									
		1350	6									
		1500	[4]6	In$_2$O$_3$ ss+Al$_2$O$_3$	C-type+corundum	Cubic+rhombohedral						
		1650	[4]2	do	do	do						
		800	20									
		1350	6									
		1700	0.0	In$_2$O$_3$ ss+unknown	C-type+unknown	Cubic+unknown					Specimen melted, unidentified phase appears to be isostructural with rhombohedral phase of Sc$_2$O$_3$–Al$_2$O$_3$ system. This phase similar to unknown phase previously reported by Keith and Roy [3].	
Sc$_2$O$_3$–Al$_2$O$_3$	66.7:33.3	1350	6									
		1650	6	Sc$_2$O$_3$ ss+(1−x)Sc$_2$O$_3$·xAl$_2$O$_3$ ss.	C-type+unknown	Cubic+rhombohedral						
	50:50	1350	6									
		1650	9.5	(1−x)Sc$_2$O$_3$·xAl$_2$O$_3$ ss	Unknown	Rhombohedral	9.45			87.4	Structure type appears to be rhombohedral distortion of fluorite type; see text.	
		1790	0.08	do	do	do						
		1960	.08	do	do	do					Specimen melted	
Fe$_2$O$_3$–Al$_2$O$_3$[3b]	53:47	800	20									
		1000	65									
		1375	[4]9	(1−x)Fe$_2$O$_3$·xAl$_2$O$_3$ ss	Kappa alumina	Orthorhombic						
	50:50	800	20									
		1000	65									
		1350	[4]6	(1−x)Fe$_2$O$_3$·xAl$_2$O$_3$ ss	Kappa alumina	Orthorhombic						
		1450		(1−x)Fe$_2$O$_3$·xAl$_2$O$_3$ ss	Kappa alumina	Orthorhombic	7.03	6.33	7.411		This cell apparently not correct; see text.	Richardson, Ball and Rigby [20].
	47:53	800	20									
		1000	65									
		1350	[4]6	(1−x)Fe$_2$O$_3$·xAl$_2$O$_3$ ss	Kappa alumina	Orthorhombic	8.59	9.23	4.98			
Cr$_2$O$_3$–Al$_2$O$_3$[3c]	50:50	1000	6									
		1600	6	(1−x)Cr$_2$O$_3$·xAl$_2$O$_3$ ss	Corundum	Rhombohedral						
Ga$_2$O$_3$–Al$_2$O$_3$[4d]	50:50	1350	6									
		1650	6	Ga$_2$O$_3$ ss	Beta gallia	Monoclinic						
	30:70	1350	6									
		1650	6	Ga$_2$O$_3$ ss+Al$_2$O$_3$ ss	Beta gallia+Corundum	Monoclinic+rhombohedral.						

Ga^{+3} and larger cations

System	Composition	Heat treatment Temp.	Time	Phases identified by X-ray diffraction	Structure type	Symmetry	a	b	c	α	Remarks	References
La$_2$O$_3$–Ga$_2$O$_3$	66.7:33.3	1350	6									
		1500	[4]2	2La$_2$O$_3$·Ga$_2$O$_3$	Unknown	Unknown					May be small amount of perovskite type compound present.	
	50:50			La$_2$O$_3$·Ga$_2$O$_3$	Perovskite	Orthorhombic	5.496	5.524	7.787		Orthorhombic to rhombohedral transformation occurs at 875 °C [6].	Geller [6].
	8.2:91.8	1000	20									
		1350	6	La$_2$O$_3$·Ga$_2$O$_3$+Ga$_2$O$_3$	Perovskite+beta gallia	Orthorhombic+monoclinic.						
Pr$_2$O$_3$–Ga$_2$O$_3$	50:50			Pr$_2$O$_3$·Ga$_2$O$_3$	Perovskite	Orthorhombic	5.465	5.495	7.729			Geller [6].
Nd$_2$O$_3$–Ga$_2$O$_3$	75:25	1350	6									
		1500	6	Nd$_2$O$_3$+2Nd$_2$O$_3$·Ga$_2$O$_3$	A-type+unknown	Hexagonal+unknown					Specimen partially melted	
	66.7:33.3	1350	6									
		1500	6	Nd$_2$O$_3$+2Nd$_2$O$_3$·Ga$_2$O$_3$+Nd$_2$O$_3$·Ga$_2$O$_3$.	A-Type+unknown+perovskite.	Hexagonal+unknown+orthorhombic.					Nonequilibrium	

System	Ratio	Temp	Time	Composition	Phase	Structure	a	b	c	Remarks	Reference
		1575	6	$2Nd_2O_3 \cdot Ga_2O_3$	Unknown	Unknown					
	50:50			$Nd_2O_3 \cdot Ga_2O_3$	Perovskite	Orthorhombic	5.426	5.502	7.706		Geller [6].
	40:60	1000	6								
		1350	[4]6	$Nd_2O_3 \cdot Ga_2O_3$ + $3Nd_2O_3 \cdot 5Ga_2O_3$	Perovskite+garnet	Orthorhombic+cubic	12.505			Listed dimension for garnet phase in mixture.	
	37.5:62.5	1000	6								
		1350	6								
		1500	[4]6	$3Nd_2O_3 \cdot 5Ga_2O_3$	Garnet	Cubic	12.505				
Sm_2O_3–Ga_2O_3	75:25	1350	6								
		1500	6	$3Sm_2O_3 \cdot Ga_2O_3$ + $2Sm_2O_3 \cdot Ga_2O_3$	Unknown+unknown	Unknown+unknown				Nonequilibrium	
		1575	6	$3Sm_2O_3 \cdot Ga_2O_3$	Unknown	Unknown					
	50:50	1350	6								
		1500	6	$2Sm_2O_3 \cdot Ga_2O_3$ + $3Sm_2O_3 \cdot 5Ga_2O_3$ $_{ss}$	Unknown+garnet	Unknown+cubic	12.448			Listed dimension for garnet phase in mixture.	
	40:60	1000	20								
		1350	6								
		1500	[4]4	$2Sm_2O_3 \cdot Ga_2O_3$ + $3Sm_2O_3 \cdot 5Ga_2O_3$ $_{ss}$	Unknown+garnet	Unknown+cubic	12.448			Listed dimension for garnet phase in mixture.	
	37.5:62.5	1000	6								
		1350	6								
		1500	[4]6	$3Sm_2O_3 \cdot 5Ga_2O_3$	Garnet	Cubic	12.434				
Eu_2O_3–Ga_2O_3	75:25	1350	6								
		1500	6	$3Eu_2O_3 \cdot Ga_2O_3$ + $2Eu_2O_3 \cdot Ga_2O_3$	Unknown+unknown	Unknown+unknown					
		1575	6	$3Eu_2O_3 \cdot Ga_2O_3$	Unknown	Unknown					
	50:50	1350	6								
		1500	6	$2Eu_2O_3 \cdot Ga_2O_3$ + $3Eu_2O_3 \cdot 5Ga_2O_3$ $_{ss}$	Unknown+garnet	Unknown+Cubic	12.431			Listed dimension for garnet phase in mixture.	
	40:60	1000	6								
		1350	6								
		1500	[4]4	$3Eu_2O_3 \cdot 5Ga_2O_3$ $_{ss}$	Garnet	Cubic	12.422				
	37.5:62.5	1000	6								
		1350	6								
		1500	[4]6	$3Eu_2O_3 \cdot 5Ga_2O_3$	Garnet	Cubic	12.403				
Gd_2O_3–Ga_2O_3	75:25	1350	6								
		1500	6	$3Gd_2O_3 \cdot Ga_2O_3$	Unknown	Unknown					
		1600	6	$3Gd_2O_3 \cdot Ga_2O_3$	Unknown	Unknown					
	50:50	1350	6								
		1500	6	$3Gd_2O_3 \cdot Ga_2O_3$ + $3Gd_2O_3 \cdot 5Ga_2O_3$ $_{ss}$	Unknown+garnet	Unknown+cubic	12.426			Listed dimension for garnet phase in mixture.	
	40:60	1000	6								
		1350	6								
		1500	[4]4	$3Gd_2O_3 \cdot 5Ga_2O_3$ $_{ss}$	Garnet	Cubic	12.416				
	37.5:62.5	1000	6								
		1350	6								
		1500	[4]6	$3Gd_2O_3 \cdot 5Ga_2O_3$	Garnet	Cubic	12.377				
Dy_2O_3–Ga_2O_3	75:25	1350	6								
		1500	6	$3Dy_2O_3 \cdot Ga_2O_3$	Unknown	Unknown					
		1600	6	Dy_2O_3 + $3Dy_2O_3 \cdot Ga_2O_3$	C-type+unknown	Cubic+unknown				Nonequilibrium; the 3:1 phase apparently is decomposing.	
		1650	6	----do----	----do----	----do----				----do----	
	66.7:33.3	1350	6								
		1500	6	$3Dy_2O_3 \cdot Ga_2O_3$ + $3Dy_2O_3 \cdot 5Ga_2O_3$	Unknown+garnet	Unknown+cubic					
	50:50	1350	6								
		1500	6	$3Dy_2O_3 \cdot Ga_2O_3$ + $3Dy_2O_3 \cdot 5Ga_2O_3$ $_{ss}$	Unknown+garnet	Unknown+cubic	12.417			Listed dimension for garnet phase in mixture	
	40:60	1000	6								
		1350	6								
		1500	[4]4	$3Dy_2O_3 \cdot 5Ga_2O_3$ $_{ss}$	Garnet	Cubic	12.349				
	37.5:62.5	1000	6								
		1350	6								
		1500	[4]6	$3Dy_2O_3 \cdot 5Ga_2O_3$	Garnet	Cubic	12.308				
Ho_2O_3–Ga_2O_3	75:25	1350	6								
		1500	6	$*Ho_2O_3$ + $3Ho_2O_3 \cdot Ga_2O_3$	C-type+unknown	Cubic+unknown				Nonequilibrium	
		1600	6	----do----	----do----	----do----				----do----	
		1650	6	----do----	----do----	----do----				----do----	
	66.7:33.3	1350	6								
		1500	6	$3Ho_2O_3 \cdot Ga_2O_3$ + $3Ho_2O_3 \cdot 5Ga_2O_3$ $_{ss}$	Unknown+garnet	Unknown+cubic					
	50:50	1350	6								
		1500	6	$3Ho_2O_3 \cdot Ga_2O_3$ + $3Ho_2O_3 \cdot 5Ga_2O_3$ $_{ss}$	Unknown+garnet	Unknown+cubic	12.408			Listed dimension for garnet phase in mixture.	
	40:60	1000	6								
		1350	6								
		1500	[4]4	$3Ho_2O_3 \cdot 5Ga_2O_3$ $_{ss}$	Garnet	Cubic	12.324				

See footnotes at end of table.

358

System	Composition	Heat [1] treatment		Phases identified by X-ray diffraction	Structure type	Symmetry	Unit cell dimensions				Remarks	References [2]
		Temp.	Time				a	b	c	α		
	Mole %	°C	hr				A	A	A	deg		
	37.5:62.5	1000	6									
		1350	6									
		1500	[4] 6	3Ho$_2$O$_3$·5Ga$_2$O$_3$	Garnet	Cubic	12.282					
Y$_2$O$_3$–Ga$_2$O$_3$	75:25	1350	6									
		1500	6	Y$_2$O$_3$+3Y$_2$O$_3$·Ga$_3$O$_3$+ 3Y$_2$O$_3$·5Ga$_2$O$_3$ ss	C-type+unknown+ garnet.	Cubic+unknown+ cubic					Nonequilibrium	
		1600	6	___do___	___do___	___do___					___do___	
		1650	6	___do___	___do___	___do___					___do___	
	66.7:33.3	1350	6									
		1500	6	3Y$_2$O$_3$·Ga$_2$O$_3$+ 3Y$_2$O$_3$·5Ga$_2$O$_3$ ss	Unknown+garnet	Unknown+cubic						
	50:50	1350	6									
		1500	6	3Y$_2$O$_3$·Ga$_2$O$_3$+ 3Y$_2$O$_3$·5Ga$_2$O$_3$ ss	Unknown+garnet	Unknown+cubic	12.441				Listed dimension for garnet phase in mixture.	
		1600	6	___do___	___do___	___do___						
	40:60	1000	6									
		1350	6									
		1500	[4] 4	3Y$_2$O$_3$·5Ga$_2$O$_3$ ss	Garnet	Cubic	12.318					
	37.5:62.5	1000	6									
		1350	6									
		1500	[4] 6	3Y$_2$O$_3$·5Ga$_2$O$_3$	Garnet	Cubic	12.275					
Er$_2$O$_3$–Ga$_2$O$_3$	90:10	1350	6									
		1500	6	Er$_2$O$_3$+3Er$_2$O$_3$·Ga$_2$O$_3$	C-type+unknown	Cubic+unknown						
	80:20	1350	6									
		1500	6	Er$_2$O$_3$+3Er$_2$O$_3$·Ga$_2$O$_3$	C-type+unknown	Cubic+unknown						
		1620	1.3	___do___	___do___	___do___						
		1350	6									
		1500	6									
		1750	.08									
		1625	.25	Er$_2$O$_3$+3Er$_2$O$_3$· 5Ga$_2$O$_3$ ss	C-type+garnet	Cubic+cubic					Specimen melted; then annealed	
	75:25	1350	6									
		1500	6	Er$_2$O$_3$+Er$_2$O$_3$·Ga$_2$O$_3$ +3Er$_2$O$_3$·5Ga$_2$O$_3$	C-type+unknown+ garnet	Cubic+unknown+ cubic					Nonequilibrium	
		1600	6	Er$_2$O$_3$+3Er$_2$O$_3$·Ga$_2$O$_3$	C-type+unknown	Cubic+unknown					Nonequilibrium; C-type phase considerably reduced in amount relative to previous heat.	
		1650	6	___do___	___do___	___do___					Nonequilibrium; C-type phase increased in amount relative to previous heat.	
		1350	6									
		1500	6									
		1745	.08									
		1700	.5	Er$_2$O$_3$+3Er$_2$O$_3$· 5Ga$_2$O$_3$ ss	C-type+garnet	Cubic+cubic					Specimen melted; then annealed	
	50:50	1350	6									
		1500	6	3Er$_2$O$_3$·Ga$_2$O$_3$+ 3Er$_2$O$_3$·5Ga$_2$O$_3$ ss	Unknown+garnet	Unknown+cubic	12.400				Listed dimension for garnet phase in mixture.	
		1645	.5	___do___	___do___	___do___						
		1350	6									
		1500	6									
		1745	.08									
		1635	.25	Er$_2$O$_3$+3Er$_2$O$_3$· 5Ga$_2$O$_3$ ss	C-type+garnet	Cubic+cubic					Specimen melted; then annealed	
	40:60	1000	6									
		1350	6									
		1500	[4] 4	3Er$_2$O$_3$·5Ga$_2$O$_3$ ss	Garnet	Cubic	12.300					
	37.5:62.5	1000	6									
		1350	6									
		1500	[4] 6	3Er$_2$O$_3$·5Ga$_2$O$_3$	Garnet	Cubic	12.254					
Tm$_2$O$_3$–Ga$_2$O$_3$	50:50	1350	6									
		1500	6	Tm$_2$O$_3$+3Tm$_2$O$_3$· 5Ga$_2$O$_3$ ss	C-type+garnet	Cubic+cubic	12.369				Listed dimension for garnet phase in mixture.	

System	Ratio	Temp	Time	Compound	Phase	Crystal system	a	b	c	Remarks	Reference
Yb_2O_3–Ga_2O_3	50:50	1350	6								
		1500	6	Yb_2O_3+$3Yb_2O_3$·$5Ga_2O_3$ ss	C-type+garnet	Cubic+cubic	12.344			Listed dimension for garnet phase in mixture.	
	40:60	1000	6								
		1350	6								
		1500	4 4	$3Yb_2O_3$·$5Ga_2O_3$ ss	Garnet	Cubic	12.232				
	37.5:62.5	1000	6								
		1350	6								
		1500	4 6	$3Yb_2O_3$·$5Ga_2O_3$	Garnet	Cubic	12.200				
Lu_2O_3–Ga_2O_3	50:50	1350	6								
		1500	6	Lu_2O_3+$3Lu_2O_3$·$5Ga_2O_3$ ss	C-type+garnet	Cubic+cubic	12.320			Listed dimension for garnet phase in mixture.	
	40:60	1000	6								
		1350	6								
		1500	4 4	$3Lu_2O_3$·$5Ga_2O_3$ ss	Garnet	Cubic	12.231				
	37.5:62.5	1000	6								
		1350	6								
		1500	4 6	$3Lu_2O_3$·$5Ga_2O_3$	Garnet	Cubic	12.183				
In_2O_3–Ga_2O_3[3e]	50:50	800	20								
		1400	4 6								
		1450	4 6	$(1-x)In_2O_3$·xGa_2O_3 ss	Unknown	Unknown				Similar to kappa alumina type phases.	
Sc_2O_3–Ga_2O_3	66.7:33.3	1350	6								
		1500	6	$Sc_2O_{3\ ss}$+$(1-x)Sc_2O_3$·xGa_2O_3 ss	C-type+unknown	Cubic+unknown					
	50:50	1350	6								
		1500	6								
		1650	6	$Sc_2O_{3\ ss}$+$(1-x)Sc_2O_3$·xGa_2O_3 ss	C-type+unknown	Cubic+unknown					
	37.5:62.5	1350	6								
		1500	6								
		1650	6	$(1-x)Sc_2O_3$·xGa_2O_3 ss	Unknown	Unknown				Unknown phase similar to kappa alumina type phases. It also appears to be isostructural with $(1-x)In_2O_3$·xGa_2O_3 ss	
	33.3:66.7	1350	6								
		1500	6								
		1650	6	$(1-x)Sc_2O_3$·xGa_2O_3 ss	Unknown	Unknown					
Fe_2O_3–Ga_2O_3	~50:50	--------	--------	$(1-x)Fe_2O_3$·xGa_2O_3 ss $(x\sim.5)$	Unknown	Orthorhombic	8.75	9.40	5.07		Wood [21].
	50:50	800	20								
		1000	65								
		1300	6	$(1-x)Fe_2O_3$·xGa_2O_3 ss	Kappa alumina	Orthorhombic	8.73	9.38	5.08	Same phase as reported by Wood [2].	
		1500	6	$Fe_3O_{4\ ss}$+$Ga_2O_{3\ ss}$	Spinel+beta gallia	Cubic+monoclinic					
Cr_2O_3–Ga_2O_3	50:50	800	6								
		1000	6								
		1600	6	$Cr_2O_{3\ ss}$+$Ga_2O_{3\ ss}$	Corundum+beta gallia.	Rhombohedral+monoclinic.					
	33.3:66.7	800	20								
		1350	6								
		1500	6	$Cr_2O_{3\ ss}$+$Ga_2O_{3\ ss}$	Corundum+beta gallia.	Rhombohedral+monoclinic.					
	20:80	800	20								
		1350	6								
		1500	6	$Ga_2O_{3\ ss}$	Beta gallia	Monoclinic.					

Cr^{+3} and larger cations

System	Ratio	Temp	Time	Compound	Phase	Crystal system	a	b	c	Remarks	Reference
La_2O_3–Cr_2O_3	50:50	--------	--------	La_2O_3·Cr_2O_3	Perovskite	Orthorhombic	5.477	5.514	7.755		Geller [6].
Pr_2O_3–Cr_2O_3	50:50	--------	--------	Pr_2O_3·Cr_2O_3	Perovskite	Orthorhombic	5.444	5.484	7.710		Geller [6].
Nd_2O_3–Cr_2O_3	50:50	--------	--------	Nd_2O_3·Cr_2O_3	Perovskite	Orthorhombic	5.412	5.494	7.695		Geller [6].
Sm_2O_3–Cr_2O_3	66.7:33.3	800	20								
		1350	6								
		1500	6	Sm_2O_3+Sm_2O_3·Cr_2O_3	B-type+perovskite	Monoclinic+orthorhombic.					
	50:50	--------	--------	Sm_2O_3·Cr_2O_3	Perovskite	Orthorhombic	5.372	5.502	7.650	Results confirmed in present work for specimen heat treated at 1600 °C.	Geller [6].
	37.5:62.5	800	20								
		1350	6								
		1500	6	Sm_2O_3·Cr_2O_3+Cr_2O_3	Perovskite+corundum	Orthorhombic+rhombohedral					
Eu_2O_3–Cr_2O_3	50:50	1000	6								
		1600	6	Eu_2O_3·Cr_2O_3	Perovskite	Orthorhombic	5.33	7.61	5.50		

See footnotes at end of table.

TABLE 1.—*Binary oxide mixtures of the trivalent cations*—Continued

Cr^{+3} and larger cations—Continued

System	Composition	Heat[1] treatment		Phases identified by X-ray diffraction	Structure type	Symmetry	Unit cell dimensions				Remarks	References[2]
		Temp.	Time				a	b	c	α		
	Mole %	°C	hr				A	A	A	deg		
Gd$_2$O$_3$–Cr$_2$O$_3$	66.7:33.3	800	20									
		1350	6									
		1500	6	Gd$_2$O$_3$+Gd$_2$O$_3$·Cr$_2$O$_3$	B-type+perovskite	Monoclinic+ortho-rhombic						Geller [6].
	50:50	--------	--------	Gd$_2$O$_3$·Cr$_2$O$_3$	Perovskite	Orthorhombic	5.312	5.514	7.611		Results confirmed in present work for specimen heat treated at 1600 °C.	
	37.5:62.5	800	20									
		1350	6									
		1500	6	Gd$_2$O$_3$·Cr$_2$O$_3$+Cr$_2$O$_3$	Perovskite+corundum	Orthorhombic+rhombohedral						
Dy$_2$O$_3$–Cr$_2$O$_3$	50:50	1000	6									
		1600	6	Dy$_2$O$_3$·Cr$_2$O$_3$	Perovskite	Orthorhombic	5.26	7.50	5.51			
Y$_2$O$_3$–Cr$_2$O$_3$	50:50	--------	--------	Y$_2$O$_3$·Cr$_2$O$_3$	Perovskite	Orthorhombic	5.247	5.518	7.540			Geller [6].
Er$_2$O$_3$–Cr$_2$O$_3$	50:50	1000	6									
		1600	6	Er$_2$O$_3$·Cr$_2$O$_3$	Perovskite	Orthorhombic	5.22	7.51	5.51			
Yb$_2$O$_3$–Cr$_2$O$_3$	66.7:33.3	800	20									
		1350	6									
		1500	6	Yb$_2$O$_3$+Yb$_2$O$_3$·Cr$_2$O$_3$	C-type+perovskite	Cubic+orthorhombic						
	50:50	1000	6									
		1600	6	Yb$_2$O$_3$·Cr$_2$O$_3$	Perovskite	Orthorhombic	5.18	7.51	5.49			
	37.5:62.5	800	20									
		1350	6									
		1500	6	Yb$_2$O$_3$·Cr$_2$O$_3$+Cr$_2$O$_3$	Perovskite+corundum	Orthorhombic+rhombohedral						
Lu$_2$O$_3$–Cr$_2$O$_3$	50:50	1000	6									
		1600	6	Lu$_2$O$_3$·Cr$_2$O$_3$	Perovskite	Orthorhombic	5.17	7.46	5.49			
In$_2$O$_3$–Cr$_2$O$_3$	50:50	1000	6									
		1600	[4] 6	In$_2$O$_3$ ss+Cr$_2$O$_3$ ss	C-type+corundum	Cubic+rhombohedral						
Sc$_2$O$_3$–Cr$_2$O$_3$	80:20	800	20									
		1350	6									
		1500	6	Sc$_2$O$_3$ ss+(1−x)Sc$_2$O$_3$·xCr$_2$O$_3$ ss	C-type+unknown	Cubic+unknown						
	75:25	800	6									
		1350	6									
		1500	6	(1−x)Sc$_2$O$_3$·xCr$_2$O$_3$ ss	Unknown	Unknown					Unknown phase similar to kappa alumina type phase.	
	66.7:33.3	800	20									
		1600	6	(1−x)Sc$_2$O$_3$·xCr$_2$O$_3$ ss+Cr$_2$O$_3$ ss	Unknown+corundum	Unknown+rhombohedral						
Sc$_2$O$_3$–Cr$_2$O$_3$	50:50	1000	20									
		1600	6	(1−x)Sc$_2$O$_3$·xCr$_2$O$_3$ ss+Cr$_2$O$_3$ ss	Unknown+corundum.	Unknown+rhombohedral.						
Fe$_2$O$_3$–Cr$_2$O$_3$ [3f]	50:50	1000	6									
		1350	6	(1−x)Fe$_2$O$_3$·xCr$_2$O$_3$ ss	Corundum	Rhombohedral						

Fe^{+3} and larger cations

System	Composition	Heat[1] treatment		Phases identified by X-ray diffraction	Structure type	Symmetry	Unit cell dimensions				Remarks	References[2]
		Temp.	Time				a	b	c	α		
La$_2$O$_3$–Fe$_2$O$_3$ [3g]	50:50	1500	1	La$_2$O$_3$·Fe$_2$O$_3$	Perovskite	Orthorhombic	5.545	7.851	5.562			Roth [4].
Pr$_2$O$_3$–Fe$_2$O$_3$	50:50	--------	--------	Pr$_2$O$_3$·Fe$_2$O$_3$	Perovskite	Orthorhombic	5.495	5.578	7.810			Geller and Wood [5].
Nd$_2$O$_3$–Fe$_2$O$_3$	50:50	--------	--------	Nd$_2$O$_3$·Fe$_2$O$_3$	Perovskite	Orthorhombic	5.441	5.573	7.753			Geller and Wood [5].
Sm$_2$O$_3$–Fe$_2$O$_3$	50:50	--------	--------	Sm$_2$O$_3$·Fe$_2$O$_3$	Perovskite	Orthorhombic	5.394	5.592	7.711			Geller and Wood [5].
	37.5:62.5	--------	--------	3Sm$_2$O$_3$·5Fe$_2$O$_3$	Garnet	Cubic	12.524				Garnet phase does not form stably in binary mixtures containing Fe$_2$O$_3$ and trivalent cations larger than Sm^{+3} [34].	Bertaut and Forrat [34].

System	Composition	Temp.	Time	Compound	Structure type	Crystal system	a	b	c		Remarks	Reference
$_2O_3-Fe_2O_3$	50:50	--------	--------	$Eu_2O_3\cdot Fe_2O_3$	Perovskite	Orthorhombic	5.371	5.611	7.686	--------		Geller and Wood [5].
	37.5:62.5	--------	--------	$3Eu_2O_3\cdot 5Fe_2O_3$	Garnet	Cubic	12.518					Bertaut and Forrat [34].
$Gd_2O_3-Fe_2O_3$[3h]	50:50	--------	--------	$Gd_2O_3\cdot Fe_2O_3$	Perovskite	Orthorhombic	5.346	5.616	7.668	--------	Results confirmed in present work for specimen heat treated at 1300 °C.	Geller and Wood [5].
	37.5:62.5	--------	--------	$3Gd_2O_3\cdot 5Fe_2O_3$	Garnet	Cubic	12.479					Bertaut and Forrat [34].
$Dy_2O_3-Fe_2O_3$	66.7:33.3	800	20									
		1000	20									
		1350	6	$Dy_2O_3+Dy_2O_3\cdot Fe_2O_3$	C-type+perovskite	Cubic+orthorhombic						
	50:50	800	20									
		1000	65									
		1300	6	$Dy_2O_3\cdot Fe_2O_3+$ $3Dy_2O_3\cdot 5Fe_2O_3$	Perovskite+garnet	Orthorhombic+cubic	--------				Nonequilibrium	
		1500	6	$Dy_2O_3\cdot Fe_2O_3$	Perovskite	Orthorhombic	5.30	7.62	5.59			Bertaut and Forrat [34].
	37.5:62.5	--------	--------	$3Dy_2O_3\cdot 5Fe_2O_3$	Garnet	Cubic	12.414					
$Ho_2O_3-Fe_2O_3$	50:50	800	20									
		1000	65									
		1350	6	$Ho_2O_3\cdot Fe_2O_3+$ $3Ho_2O_3\cdot 5Fe_2O_3$	Perovskite+garnet	Orthorhombic+cubic					Nonequilibrium	
		1500	6	$Ho_2O_3\cdot Fe_2O_3$	Perovskite	Orthorhombic	5.30	7.58	5.59			
	37.5:62.5	--------	--------	$3Ho_2O_3\cdot 5Fe_2O_3$	Garnet	Cubic	12.380					Bertaut and Forrat [34].
$Y_2O_3-Fe_2O_3$[3i]	50:50	1500	1	$Y_2O_3\cdot Fe_2O_3$	Perovskite	Orthorhombic	5.279	7.609	5.590			Roth [4].
	37.5:62.5			$3Y_2O_3\cdot 5Fe_2O_3$	Garnet	Cubic	12.376					Bertaut and Forrat [34].
$Er_2O_3-Fe_2O_3$	50:50	800	20									
		1000	65									
		1300	6									
		1500	6	$Er_2O_3\cdot Fe_2O_3$	Perovskite	Orthorhombic	5.26	7.58	5.58			
	37.5:62.5	--------	--------	$3Er_2O_3\cdot 5Fe_2O_3$	Garnet	Cubic	12.349					Bertaut and Forrat [34].
$Tm_2O_3-Fe_2O_3$	37.5:62.5	--------	--------	$3Tm_2O_3\cdot 5Fe_2O_3$	Garnet	Cubic	12.325					Bertaut and Forrat [34].
$Yb_2O_3-Fe_2O_3$	66.7:33.3	800	20									
		1000	20									
		1350	6	$Yb_2O_3+Yb_2O_3\cdot Fe_2O_3$	C-type+perovskite	Cubic+orthorhombic						
	50:50	800	20									
		1000	65									
		1300	6									
		1500	6	$Yb_2O_3\cdot Fe_2O_3$	Perovskite	Orthorhombic	5.22	7.56	5.58			
	37.5:62.5	--------	--------	$3Yb_2O_3\cdot 5Fe_2O_3$	Garnet	Cubic	12.291					Bertaut and Forrat [34].
$Lu_2O_3-Fe_2O_3$	50:50	800	20									
		1000	65									
		1300	6	$Lu_2O_3\cdot Fe_2O_3$	Perovskite	Orthorhombic	5.21	7.55	5.55			
		1500	6	----do	----do	----do						
	37.5:62.5	--------	--------	$3Lu_2O_3\cdot 5Fe_2O_3$	Garnet	Cubic	12.277					Bertaut and Forrat [34].
$In_2O_3-Fe_2O_3$	50:50	800	20									
		1000	65									
		1350	6	$In_2O_3{}_{ss}+Fe_2O_3{}_{ss}$	C-type+corundum	Cubic+rhombohedral						
		1500	6	----do	----do	----do						
$Sc_2O_3-Fe_2O_3$[3j]	50:50	800	20									
		1000	65									
		1350	6	$Sc_2O_3{}_{ss}+Fe_2O_3{}_{ss}$	C-type+corundum	Cubic+rhombohedral					Nonequilibrium	
		1500	6	$Sc_2O_3{}_{ss}$	C-type	Cubic						
	37.5:62.5	800	20									
		1000	20									
		1350	6	$Sc_2O_3{}_{ss}+Fe_2O_3{}_{ss}$	C-type+corundum	Cubic+rhombohedral						

						Sc^{+3} and larger cations						
$La_2O_3-Sc_2O_3$	50:50	--------	--------	$La_2O_3\cdot Sc_2O_3$	Perovskite	Orthorhombic	5.678	5.787	8.098	--------		Geller [6].
$Pr_2O_3-Sc_2O_3$	50:50	--------	--------	$Pr_2O_3\cdot Sc_2O_3$	Perovskite	Orthorhombic	5.615	5.776	8.027	--------		Geller [6].
$Nd_2O_3-Sc_2O_3$	50:50	--------	--------	$Nd_2O_3\cdot Sc_2O_3$	Perovskite	Orthorhombic	5.574	5.771	7.998	--------		Geller [6].

See footnotes at end of table.

TABLE 1.—*Binary oxide mixtures of the trivalent cations*—Continued

Sc^{+3} and larger cations—Continued

System	Composition	Heat [1] treatment		Phases identified by X-ray diffraction	Structure type	Symmetry	Unit cell dimensions				Remarks	References [2]
		Temp.	Time				a	b	c	α		
	Mole %	°C	hr				A	A	A	deg		
Sm$_2$O$_3$—Sc$_2$O$_3$	50:50	1350	6									
		1650	9.5	Sm$_2$O$_3$·Sc$_2$O$_3$	Perovskite	Orthorhombic	5.53	7.95	5.76			
Eu$_2$O$_3$—Sc$_2$O$_3$	50:50	1350	6									
		1650	9.5	Eu$_2$O$_3$·Sc$_2$O$_3$	Perovskite	Orthorhombic	5.51	7.94	5.76			
Gd$_2$O$_3$—Sc$_2$O$_3$	66.7:33.3	1350	6									
		1500	6									
		1650	6	Gd$_2$O$_3$ ss+Gd$_2$O$_3$·Sc$_2$O$_3$	B-type+perovskite	Monoclinic+ortho-rhombic						Geller [6].
	50:50			Gd$_2$O$_3$·Sc$_2$O$_3$	Perovskite	Orthorhombic	5.487	5.756	7.925		Results confirmed in present work for specimen heat treated at 1650 °C.	
	37.5:62.5	1350	6									
		1500	6	Gd$_2$O$_3$·Sc$_2$O$_3$+Sc$_2$O$_3$ ss	Perovskite+C-type	Orthorhombic+cubic						
		1650	6	___do___	___do___	___do___						
Dy$_2$O$_3$—Sc$_2$O$_3$	66.7:33.3	1350	6									
		1500	6	Dy$_2$O$_3$ ss+Dy$_2$O$_3$·Sc$_2$O$_3$	C-type+perovskite	Cubic-orthorhombic						
	50:50	1350	6									
		1650	9.5	Dy$_2$O$_3$·Sc$_2$O$_3$	Perovskite	Orthorhombic	5.43	7.89	5.71			
Ho$_2$O$_3$—Sc$_2$O$_3$	50:50	1350	6									
		1650	9.5									
		1875	0.3	Ho$_2$O$_3$ ss+Ho$_2$O$_3$·Sc$_2$O$_3$+Sc$_2$O$_3$ ss	C-type+perovskite+C-type	Cubic+orthorhombic+cubic	5.42	7.87	5.71		Nonequilibrium listed dimensions for perovskite phase in mixture.	
		1900	1	___do___	___do___	___do___					Nonequilibrium___	
		1950	1	___do___	___do___	___do___					___do___	
		2000	0.3	$(1-x)$Ho$_2$O$_3$·xSc$_2$O$_3$ ss+Ho$_2$O$_3$·Sc$_2$O$_3$	C-type+perovskite	Cubic+orthorhombic					Nonequilibrium; amount of perovskite phase small. Equilibrium probably single phase C-type solid solution.	
Y$_2$O$_3$—Sc$_2$O$_3$	50:50	1350	6									
		1650	9.5	Y$_2$O$_3$ ss+Y$_2$O$_3$·Sc$_2$O$_3$+Sc$_2$O$_3$ ss	C-type+perovskite+C-type	Cubic+orthorhombic+cubic					Nonequilibrium___	
		1890	0.3	$(1-x)$Y$_2$O$_3$·xSc$_2$O$_3$ ss	C-type	Cubic						
Er$_2$O$_3$—Sc$_2$O$_3$	50:50	1350	6									
		1650	9.5	Er$_2$O$_3$ ss+Sc$_2$O$_3$ ss	C-type+C-type	Cubic+cubic					Nonequilibrium___	
		1850	0.7	$(1-x)$Er$_2$O$_3$·xSc$_2$O$_3$ ss	C-type	Cubic						
Yb$_2$O$_3$—Sc$_2$O$_3$	50:50	1350	6									
		1650	9.5	Yb$_2$O$_3$ ss+Sc$_2$O$_3$ ss	C-type+C-type	Cubic+cubic					Nonequilibrium___	
		1850	0.3	$(1-x)$Yb$_2$O$_3$·xSc$_2$O$_3$ ss	C-type	Cubic						
Lu$_2$O$_3$—Sc$_2$O$_3$	50:50	1350	6									
		1650	9.5	$(1-x)$Lu$_2$O$_3$·xSc$_2$O$_3$ ss	C-type	Cubic						
In$_2$O$_3$—Sc$_2$O$_3$	50:50	800	20									
		1350	[4] 6	$(1-x)$In$_2$O$_3$·xSc$_2$O$_3$ ss	C-type	Cubic						

In^{+3} and larger cations

System	Composition	Heat treatment		Phases identified by X-ray diffraction	Structure type	Symmetry	Unit cell dimensions				Remarks	References
		Temp.	Time				a	b	c	α		
La$_2$O$_3$—In$_2$O$_3$	50:50	1350	0.5	La$_2$O$_3$·In$_2$O$_3$	Perovskite	Orthorhombic	5.723	8.207	5.914			Roth [4].
Nd$_2$O$_3$—In$_2$O$_3$	95:5	800	20									
		1350	6									
		1500	[4] 2	$(1-x)$Nd$_2$O$_3$·xIn$_2$O$_3$ ss	B-type	Monoclinic						
	85:15	800	20									
		1350	6									
		1500	[4] 2	$(1-x)$Nd$_2$O$_3$·xIn$_2$O$_3$ ss+Nd$_2$O$_3$·In$_2$O$_3$	B-type+perovskite	Monoclinic+ortho-rhombic						
	75:25	800	20									
		1350	6									
		1500	[4] 2	$(1-x)$Nd$_2$O$_3$·xIn$_2$O$_3$ ss+Nd$_2$O$_3$·In$_2$O$_3$	B-type+perovskite	Monoclinic+ortho-rhombic						
	66.7:33.3	800	20									

System	Composition	Temp.	Time	Phase	Structure type	Crystal system	a	b	c		Remarks	Reference
		1350	6									
		1500	[4] 2	$(1-x)Nd_2O_3 \cdot xIn_2O_3$ ss $+Nd_2O_3 \cdot In_2O_3$	B-type+perovskite	Monoclinic+ortho-rhombic.						
	50:50	1350	0.5	$Nd_2O_3 \cdot In_2O_3$	Perovskite	Orthorhombic	5.627	8.121	5.891			Roth [4].
	33.3:66.7	800	20									
		1350	6									
		1500	[4] 2	$Nd_2O_3 \cdot In_2O_3 + In_2O_3$	Perovskite+C-type	Orthorhombic+cubic						
$Sm_2O_3 - In_2O_3$	66.7:33.3	800	20									
		1350	6									
		1500	[4] 2	Sm_2O_3 ss $+Sm_2O_3 \cdot In_2O_3$	B-type+perovskite	Monoclinic+ortho-rhombic.						
	50:50	1350	0.5	$Sm_2O_3 \cdot In_2O_3$	Perovskite	Orthorhombic	5.589	8.082	5.886			Roth [4].
	33.3:66.7	800	20									
		1350	6									
		1500	[4] 2	$Sm_2O_3 \cdot In_2O_3 + In_2O_3$ ss	Perovskite+C-type	Orthorhombic+cubic						
$Eu_2O_3 - In_2O_3$[3k]	50:50	800	20									
		1350	6									
		1650	[4] 2	$Eu_2O_3 \cdot In_2O_3$	Unknown	Unknown					Pseudo hexagonal symmetry	Schneider [23].
$Gd_2O_3 - In_2O_3$	66.7:33.3	800	20									
		1350	6									
		1600	[4] 2	Gd_2O_3 ss $+Gd_2O_3 \cdot In_2O_3$	B-type+unknown	Monoclinic+un-known.						
	50:50	800	20									
		1350	6									
		1600	[4] 1	$Gd_2O_3 \cdot In_2O_3$	Unknown	Unknown					Isostructural with $Eu_2O_3 \cdot In_2O_3$	Schneider [23].
		1650	[4] 2	do	do	do						
	33.3:66.7	800	20									
		1350	6									
		1600	[4] 2	$Gd_2O_3 \cdot In_2O_3$ ss $+In_2O_2$ ss	Unknown+C-type	Unknown+cubic						
$Dy_2O_3 - In_2O_3$	95:5	800	20									
		1350	6									
		1600	[4] 2	Dy_2O_3 ss $+(1-x)Dy_2O_3 \cdot xIn_2O_3$ ss	C-type+B-type	Cubic+monoclinic						
	85:5	800	20									
		1350	6									
		1600	[4] 2	Dy_2O_3 ss $+(1-x)Dy_2O_3 \cdot xIn_2O_3$ ss	C-type+B-type	Cubic+monoclinic						
	75:25	800	20									
		1350	6									
		1600	[4] 2	$(1-x)Dy_2O_3 \cdot xIn_2O_3$ ss	B-type	Monoclinic						
	66.7:33.3	800	20									
		1350	6									
		1600	[4] 2	$(1-x)Dy_2O_3 \cdot xIn_2O_3$ ss $+Dy_2O_3 \cdot In_2O_3$ ss	B-type+unknown	Monoclinic+un-known.						
	50:50	800	20									
		1350	6									
		1600	[4] 1	$Dy_2O_3 \cdot In_2O_3$	Unknown	Unknown					Isostructural with $Eu_2O_3 \cdot In_2O_3$ [23]	Schneider [23]
		1650	[4] 3	$(1-x)Dy_2O_3 \cdot xIn_2O_3$ ss $+In_2O_3$ ss	B-type+C-type	Monoclinic+cubic						
	33.3:66.7	800	20									
		1350	6									
		1600	[4] 2	$Dy_2O_3 \cdot In_2O_3$ ss $+In_2O_3$ ss	Unknown+C-type	Unknown+cubic						
$Ho_2O_3 - In_2O_3$	50:50	800	20									
		1350	6									
		1600	[4] 1	$(1-x)Ho_2O_3 \cdot xIn_2O_3$ ss	C-type	Cubic						
$Er_2O_3 - In_2O_3$	50:50	800	20									
		1350	6									
		1600	[4] 1	$(1-x)Er_2O_3 \cdot xIn_2O_3$ ss	C-type	Cubic						
$Tm_2O_3 - In_2O_3$	50:50	800	20									
		1350	6									
		1600	[4] 1	$(1-x)Tm_2O_3 \cdot xIn_2O_3$ ss	C-type	Cubic						
$Yb_2O_3 - In_2O_3$	50:50	800	20									
		1350	6									
		1600	[4] 1	$(1-x)Yb_2O_3 \cdot xIn_2O_3$ ss	C-type	Cubic						
$Lu_2O_3 - In_2O_3$	50:50	800	20									
		1350	6									
		1600	[4] 1	$(1-x)Lu_2O_3 \cdot xIn_2O_3$ ss	C-type	Cubic						

[1] All specimens in present work slow cooled except where noted. Each heat treatment includes all previously listed lower temperature heatings given for the same composition.

[2] When no references are given, data was obtained in present investigation.

[3] The phase diagram for this system has been reported: (a) [22], (b) [10], (c) [26], (d) [27], (e) [28], (f) [10], (g) [29], (h) [22], (i) [18], (j) [30], (k) [23].
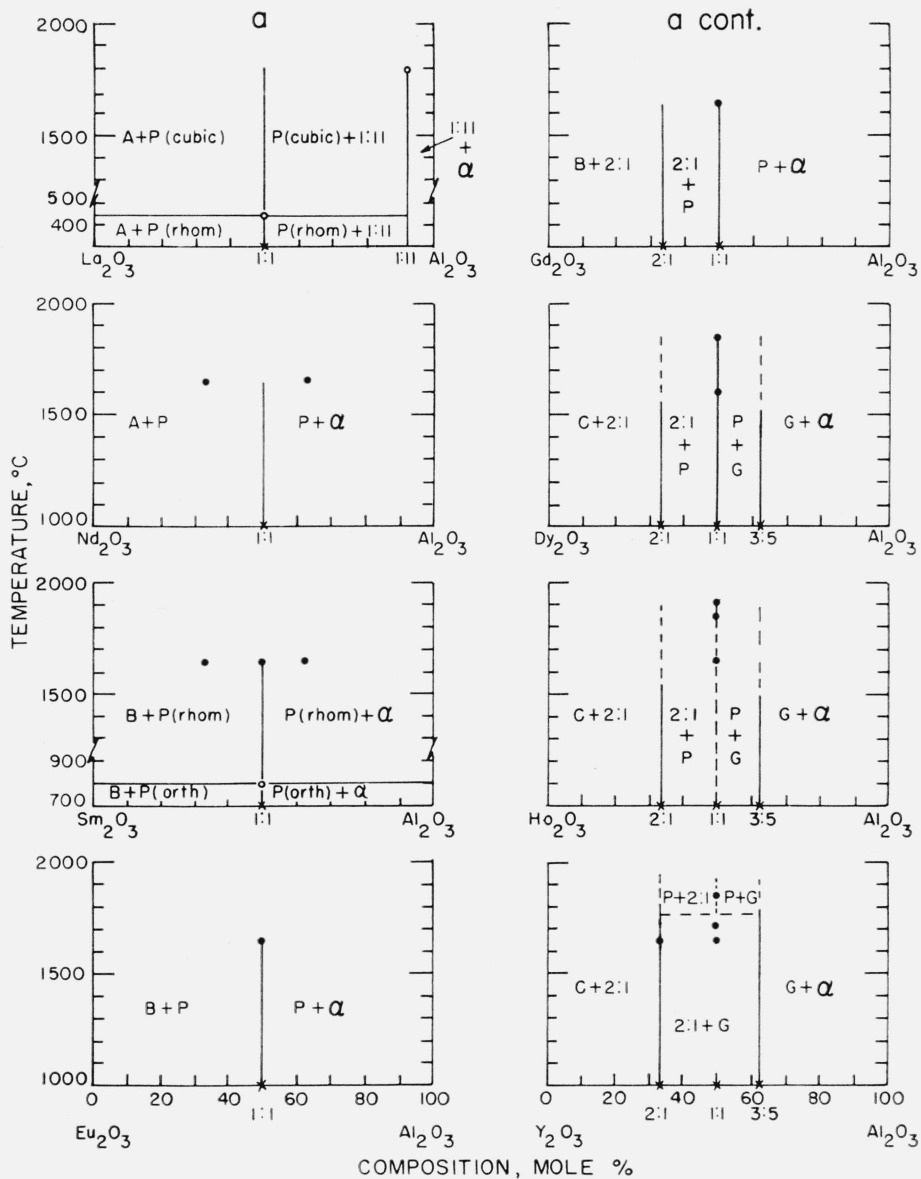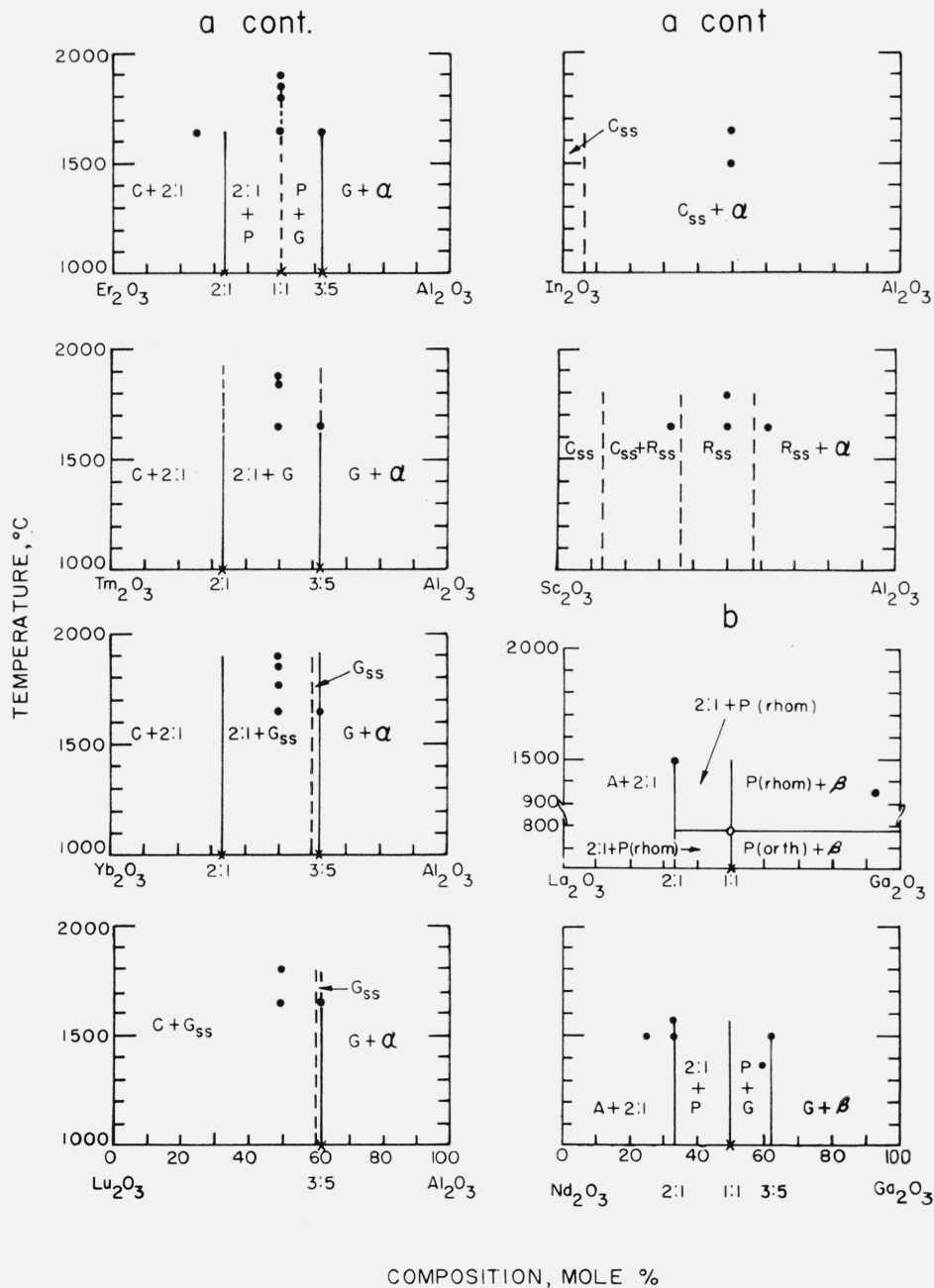
[4] Specimen heated in sealed Pt tubes and quenched.

FIGURE 5. *Predicted subsolidus binary phase diagrams for systems involving oxides of the trivalent cations*

●—compositions studied in present work
○—data taken from literature
X—data taken from literature for which no temperature of heat treatment is
   given

A—A-type rare earth oxide structure
B—B-type rare earth oxide structure
C—C-type rare earth oxide structure
G—garnet type compound
1:11—beta alumina type structure
P—perovskite type compound
R—unknown type structure, rhombohedral symmetry

S—spinel type structure
α—corundum type structure
β—beta gallia type structure
K—kappa alumina type structure
u—unknown type structure similar to kappa alumina
ss—solid solution

(a) Binary oxide systems containing Al+3 and larger cations. The following systems pertinent to this series have been previously published.

1. Y_2O_3–Al_2O_3 [22]
2. Fe_2O_3–Al_2O_3 [10]

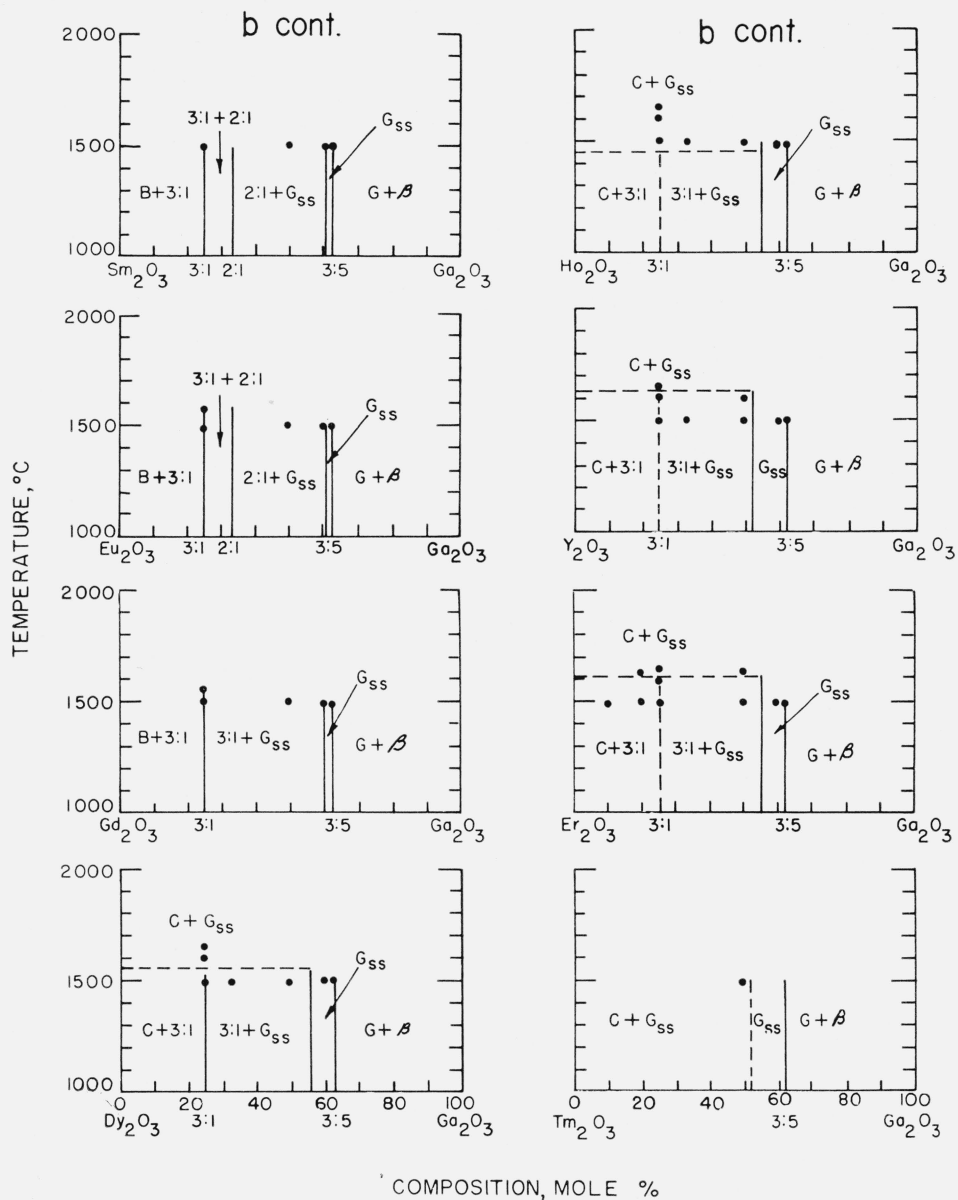3. Cr_2O_3–Al_2O_3 [26]
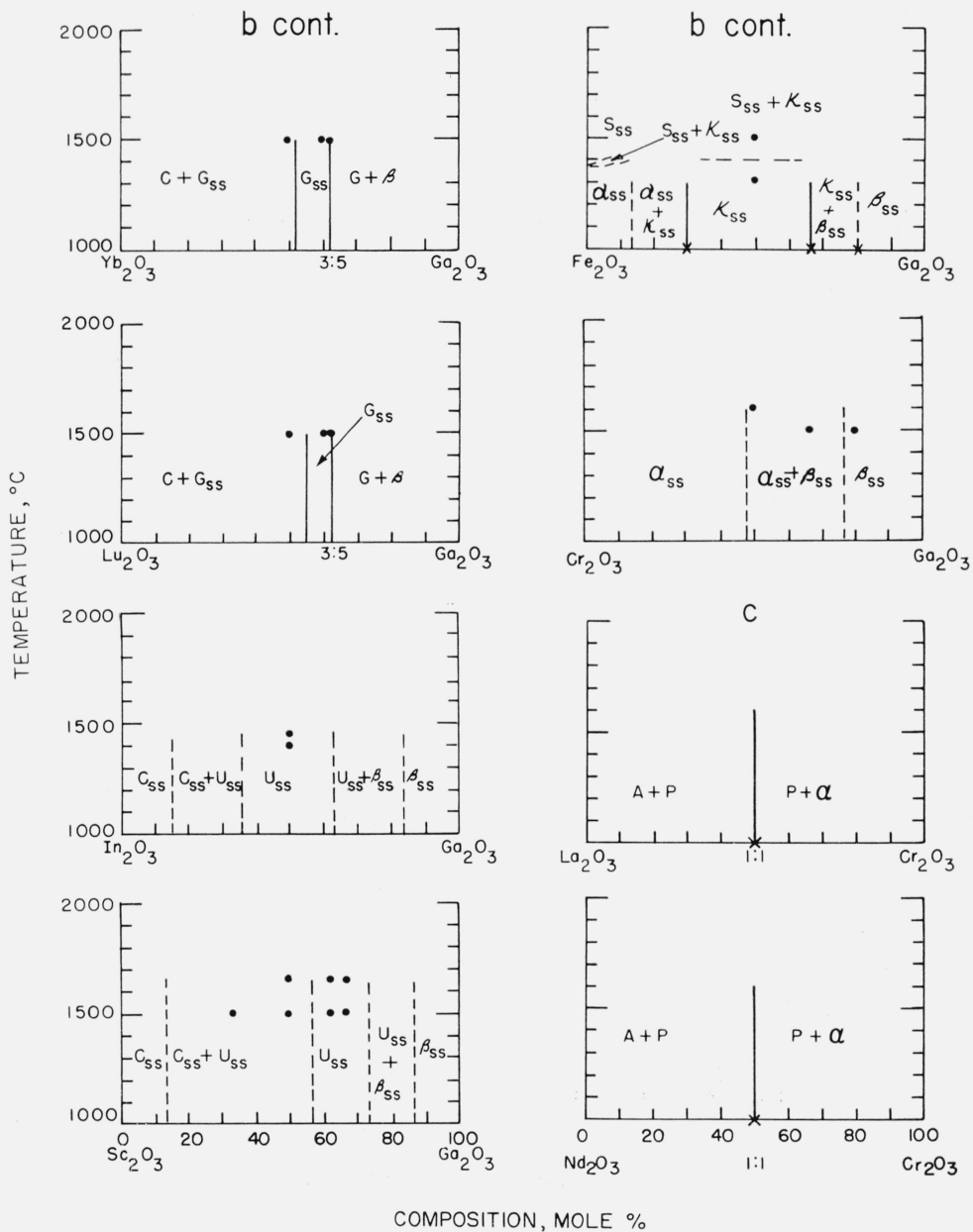4. Ga_2O_3–Al_2O_3 [27]

FIGURE 5. *Predicted subsolidus binary phase diagram for systems involving oxides of the trivalent cations*—Continued

●—compositions studied in present work
○—data taken from literature
✕—data taken from literature for which no temperature of heat treatment is given

A—A-type rare earth oxide structure
B—B-type rare earth oxide structure
C—C-type rare earth oxide structure
G—garnet type compound
1:11—beta alumina type structure
P—perovskite type compound
R—unknown type structure, rhombohedral symmetry

S—spinel type structure
α—corundum type structure
β—beta gallia type structure
K—kappa alumina type structure
u—unknown type structure similar to kappa alumina
ss—solid solution

(a) Binary oxide systems containing Al^{+3} and larger cations. The following systems pertinent to this series have been previously published.

1. Y$_2$O$_3$–Al$_2$O$_3$ [22]
2. Fe$_2$O$_3$–Al$_2$O$_3$ [10]

3. Cr$_2$O$_3$–Al$_2$O$_3$ [26]
4. Ga$_2$O$_3$–Al$_2$O$_3$ [27]

(b) Binary oxide systems containing Ga^{+3} and larger cations. The In$_2$O$_3$–Ga$_2$O$_3$ system has been previously published [28]. Boundary limits of kappa alumina solid solution taken from Remeika [35].

FIGURE 5. *Predicted subsolidus binary phase diagram for systems involving oxides of the trivalent cations*—Continued

●—compositions studied in present work
○—data taken from literature
✕—data taken from literature for which no temperature of heat treatment is
     given

A—A-type rare earth oxide structure
B—B-type rare earth oxide structure
C—C-type rare earth oxide structure
G—garnet type compound
1:11—beta alumina type structure
P—perovskite type compound
R—unknown type structure, rhombohedral symmetry

S—spinel type structure
α—corundum type structure
β—beta gallia type structure
K—kappa alumina type structure
u—unknown type structure similar to kappa alumina
ss—solid solution

(b) Binary oxide systems containing Ga⁺³ and larger cations. The In₂O₃–Ga₂O₃ system has been previously published [28]. Boundary limits of kappa alumina solid solution taken from Remeika [35].
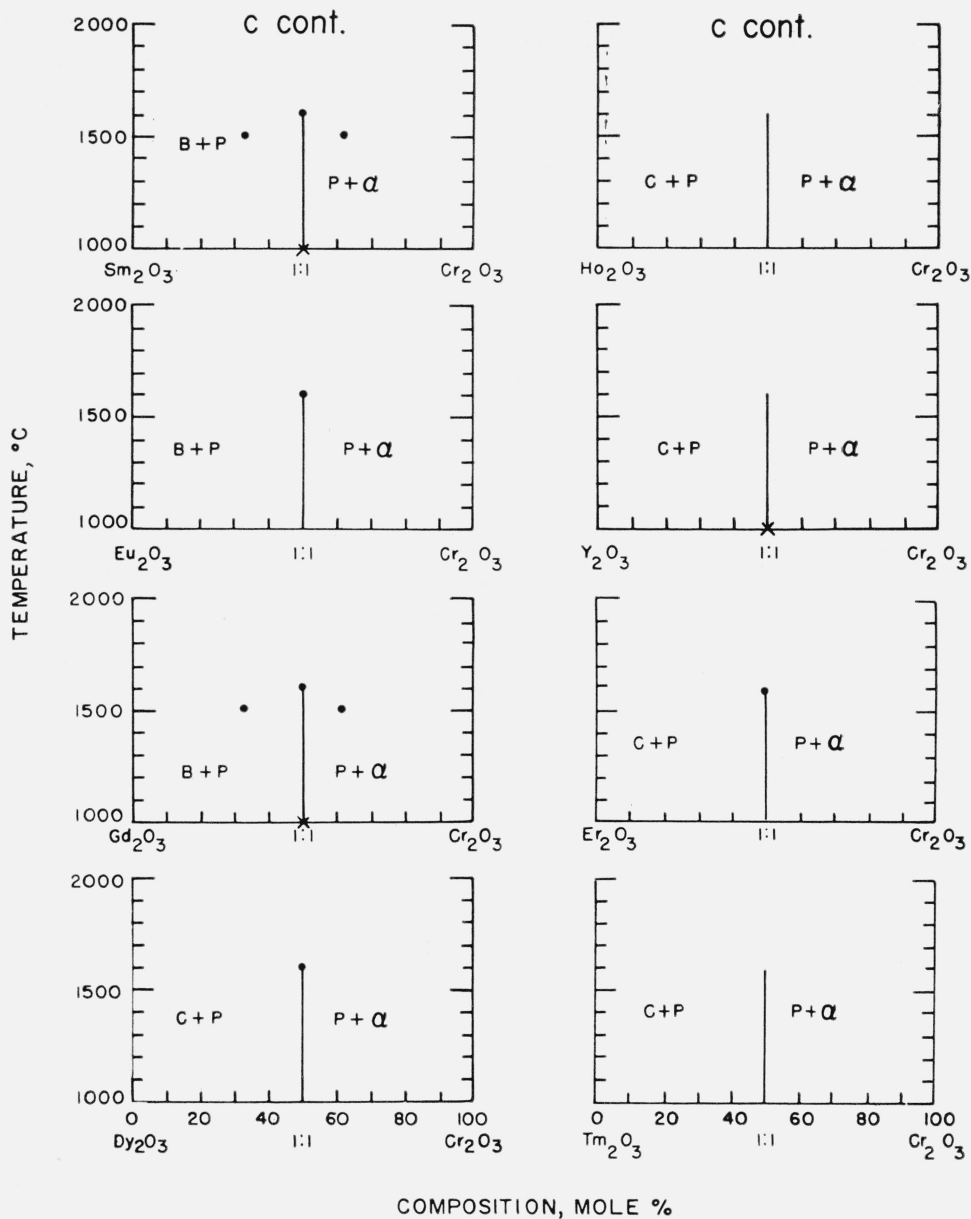
366

FIGURE 5. *Predicted subsolidus binary phase diagram for systems involving oxides of the trivalent cations*—Continued

● —compositions studied in present work
○ —data taken from literature
✕ —data taken from literature for which no temperature of heat treatment is given

A—A-type rare earth oxide structure
B—B-type rare earth oxide structure
C—C-type rare earth oxide structure
G—garnet type compound
1:11—beta alumina type structure
P—perovskite type compound
R—unknown type structure, rhombohedral symmetry

S—spinel type structure
α—corundum type structure
β—beta gallia type structure
K—kappa alumina type structure
u—unknown type structure similar to kappa alumina
ss—solid solution

(b) Binary oxide systems containing Ga⁺³ and larger cations. The In₂O₃–Ga₂O₃ system has been previously published [28]. Boundary limits of kappa alumina solid solution taken from Remeika [35].

(c) Binary oxide systems containing Cr⁺³ and larger cations. The Fe₂O₃–Cr₂O₃ system has been previously published [10].
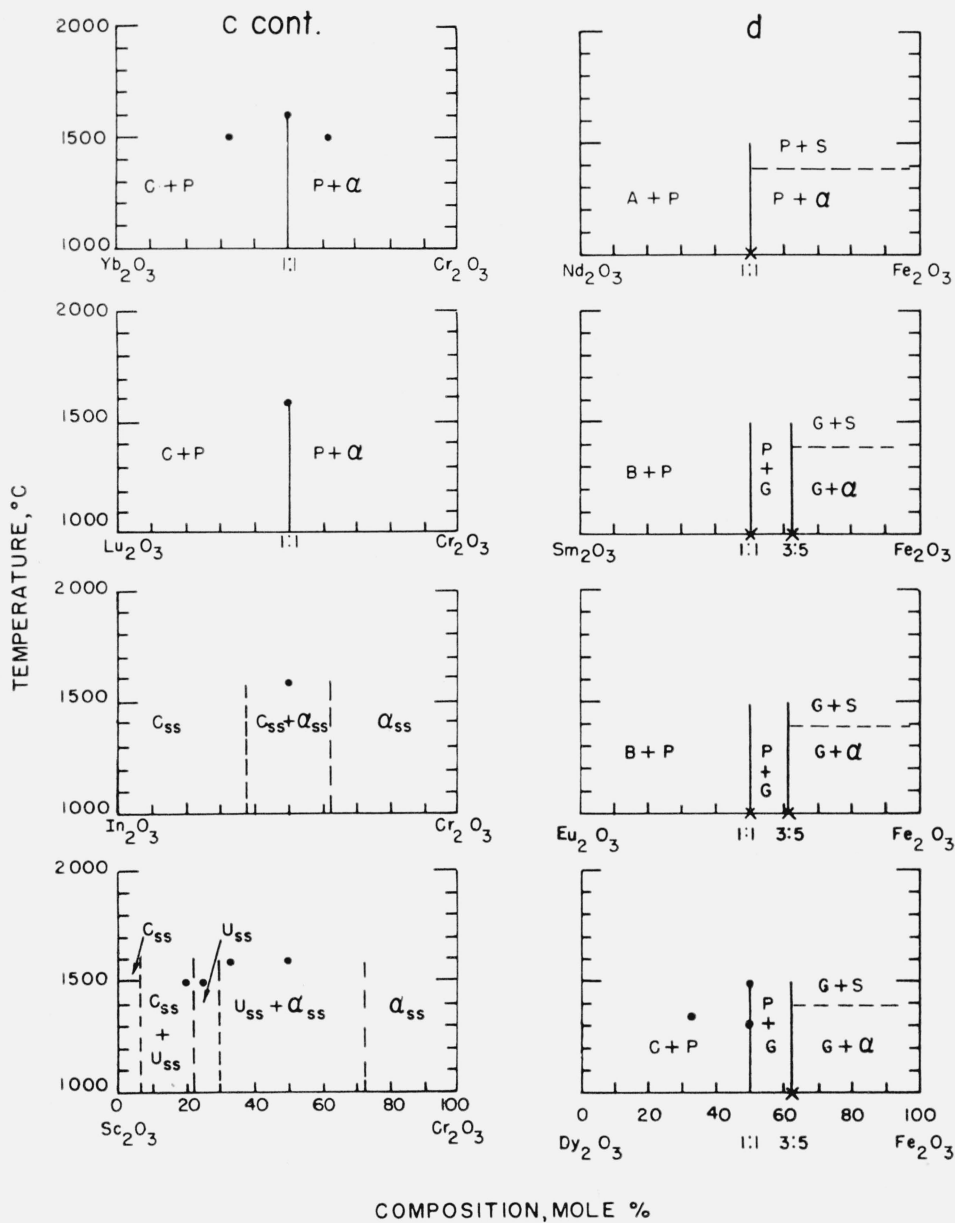
FIGURE 5. *Predicted subsolidus binary phase diagram for systems involving oxides of the trivalent cations*—Continued

● —compositions studied in present work
○ —data taken from literature
✕ —data taken from literature for which no temperature of heat treatment is given

A—A-type rare earth oxide structure
B—B-type rare earth oxide structure
C—C-type rare earth oxide structure
G—garnet type compound
1:11—beta alumina type structure
P—perovskite type compound
R—unknown type structure, rhombohedral symmetry

S—spinel type structure
α—corundum type structure
β—beta gallia type structure
K—kappa alumina type structure
u—unknown type structure similar to kappa alumina
ss—solid solution

(c) Binary oxide systems containing Cr^{+3} and larger cations. The Fe_2O_3–Cr_2O_3 system has been previously published [10].
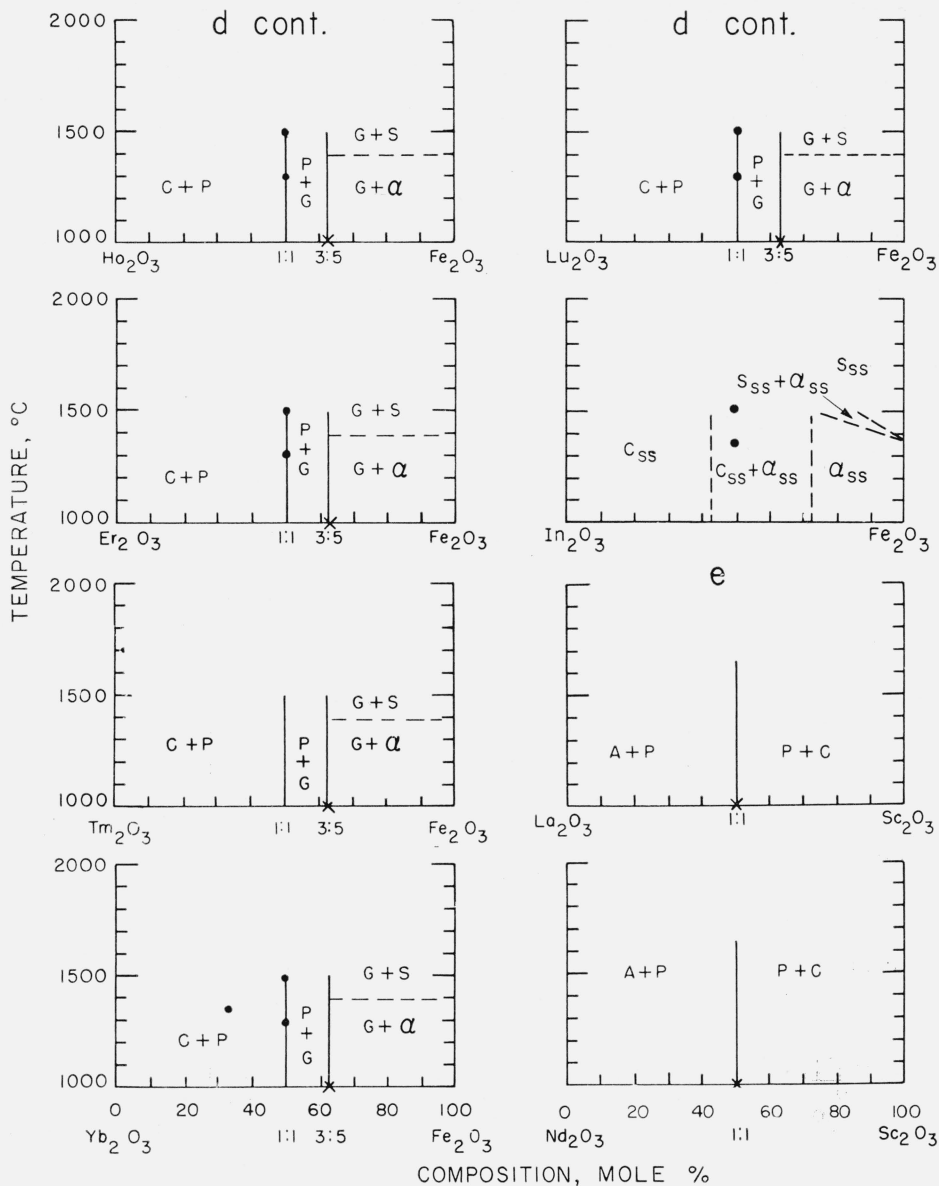
FIGURE 5. *Predicted subsolidus binary phase diagram for systems involving oxides of the trivalent cations*—Continued

● —compositions studied in present work
○ —data taken from literature
✕ —data taken from literature for which no temperature of heat treatment is given

A—A-type rare earth oxide structure
B—B- ype rare earth oxide structure
C—C-type rare earth oxide structure
G—garnet type compound
1:11—beta alumina type structure
P—perovskite type compound
R—unknown type structure, rhombohedral symmetry

S—spinel type structure
α—corundum type structure
β—beta gallia type structure
K—kappa alumina type structure
u—unknown type structure similar to kappa alumina
ss—solid solution

(c) Binary oxide systems containing Cr^{+3} and larger cations. The Fe_2O_3-Cr_2O_3 system has been previously published [10].

(d) Binary oxide systems containing Fe^{+3} and larger cations. The transformation temperature of corundum to spinel type is taken as 1390 °C. [10]. The following systems pertinent to this series have been previously published:

1. La_2O_3-Fe_2O_3 [29]
2. Gd_2O_3-Fe_2O_3 [22]

3. Y_2O_3-Fe_2O_3 [18]
4. Sc_2O_3-Fe_2O_3 [30]

FIGURE 5. *Predicted subsolidus binary phase diagram for systems involving oxides of the trivalent cations*—Continued

●—compositions studied in present work
○—data taken from literature
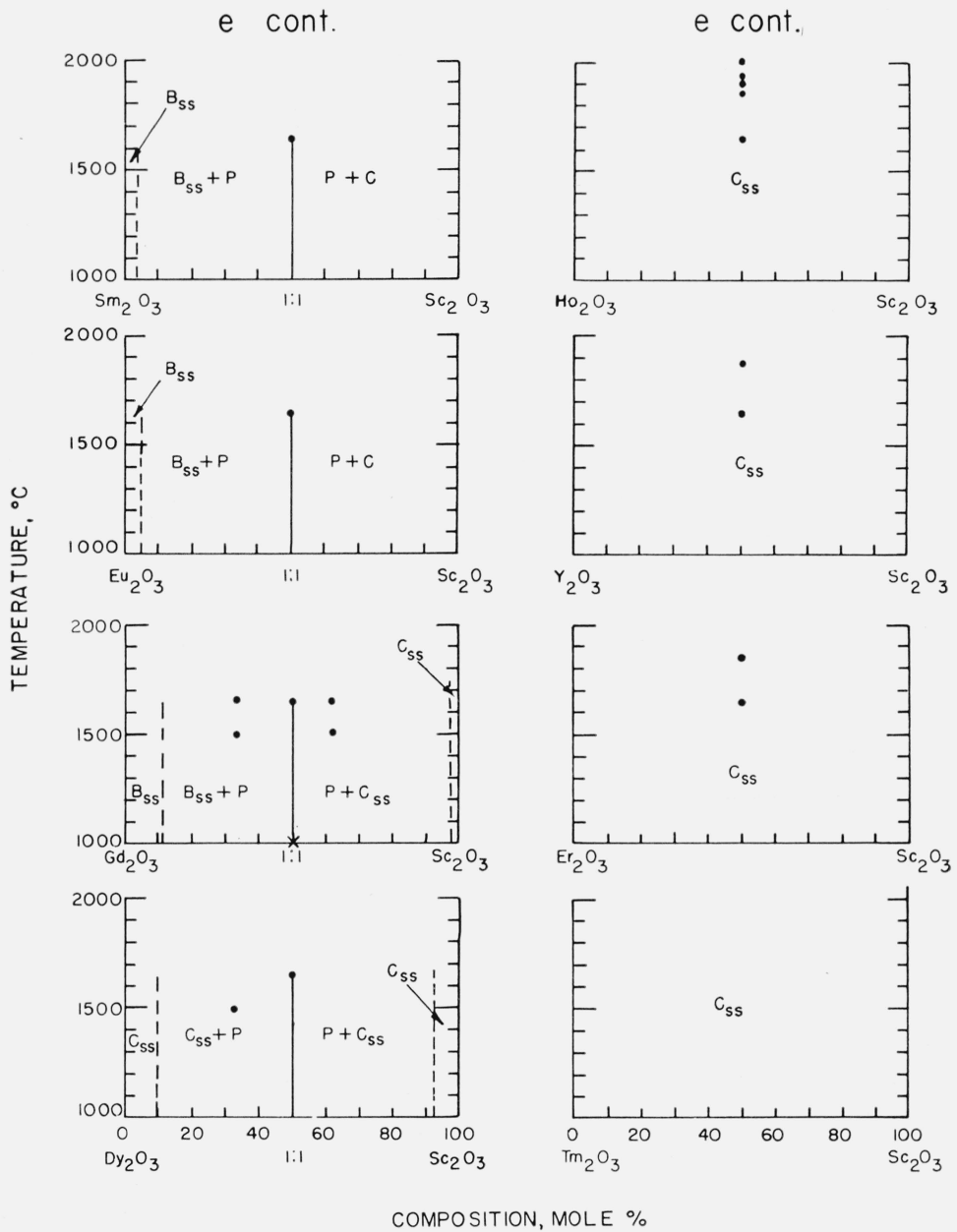✕—data taken from literature for which no temperature of heat treatment is
   given

A—A-type rare earth oxide structure
B—B-type rare earth oxide structure
C—C-type rare earth oxide structure
G—garnet type compound
1:11—beta alumina type structure
P—perovskite type compound
R—unknown type structure, rhombohedral symmetry

S—spinel type structure
α—corundum type structure
β—beta gallia type structure
K—kappa alumina type structure
u—unknown type structure similar to kappa alumina
ss—solid solution

(d) Binary oxide systems containing Fe^{+3} and larger cations. The transformation temperature of corundum to spinel type is taken as 1390 °C. [10]. The following systems pertinent to this series have been previously published:

1. La_2O_3–Fe_2O_3 [29]
2. Gd_2O_3–Fe_2O_3 [22]

3. Y_2O_3–Fe_2O_3 [18]
4. Sc_2O_3–Fe_2O_3 [30]

(e) Binary oxide systems containing Sc^{+3} and larger cations.

370

FIGURE 5. *Predicted subsolidus binary phase diagram for systems involving oxides of the trivalent cations*—Continued

●—compositions studied in present work
○—data taken from literature
×—data taken from literature for which no temperature of heat treatment is
       given

A—A-type rare earth oxide structure
B—B-type rare earth oxide structure
C—C-type rare earth oxide structure
G—garnet type compound
1:11—beta alumina type structure
P—perovskite type compound
R—unknown type structure, rhombohedral symmetry

S—spinel type structure
α—corundum type structure
β—beta gallia type structure
K—kappa alumina type structure
u—unknown type structure similar to kappa alumina
ss—solid solution

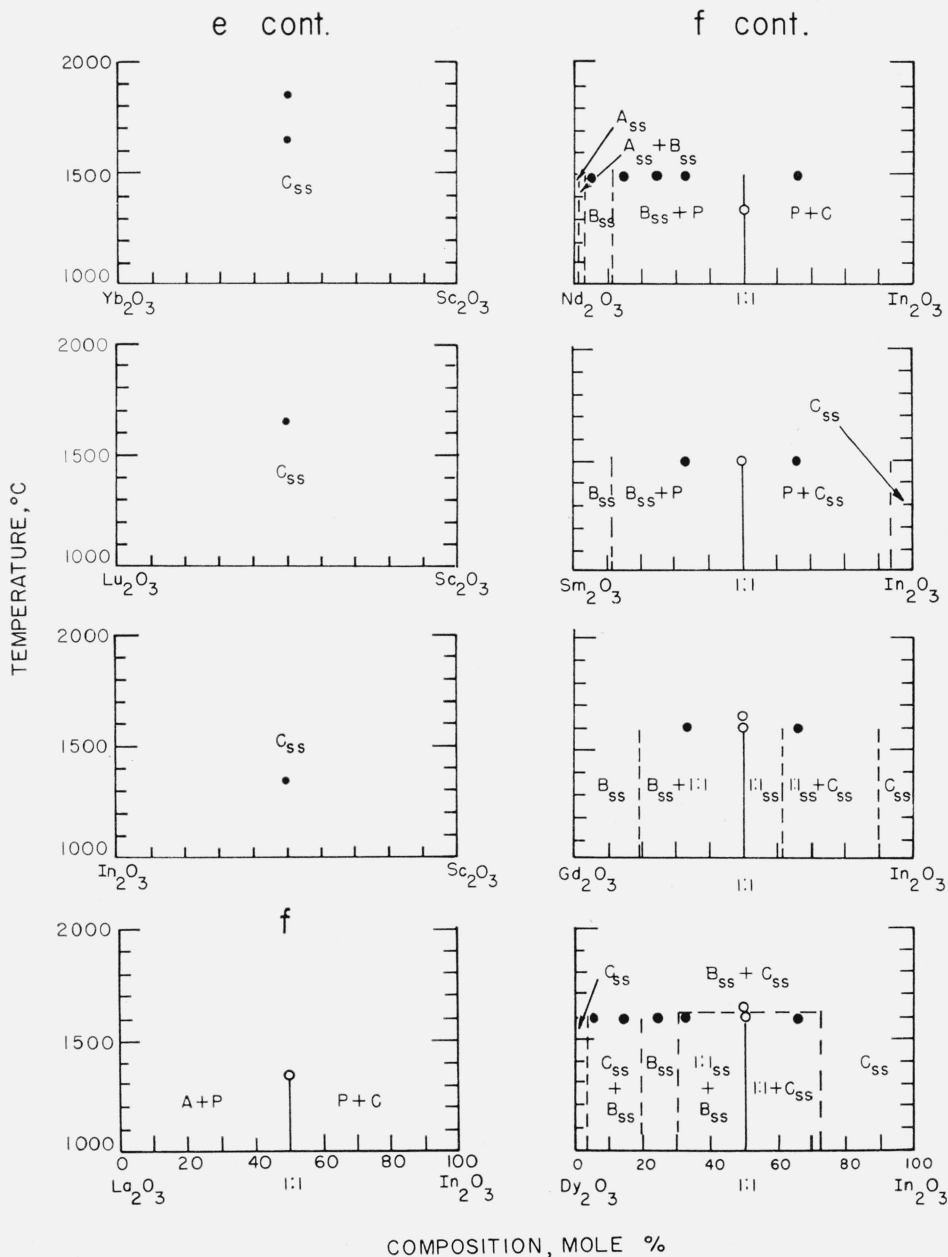(e) Binary oxide systems containing Sc⁺³ and larger cations.

FIGURE 5. *Predicted subsolidus binary phase diagram for systems involving oxides of the trivalent cations*—Continued

● —compositions studied in present work
○ —data taken from literature
✕ —data taken from literature for which no temperature of heat treatment is
given

A—A-type rare earth oxide structure
B—B-type rare earth oxide structure
C—C-type rare earth oxide structure
G—garnet type compound
1:11—beta alumina type structure
P—perovskite type compound
R—unknown type structure, rhombohedral symmetry

S—spinel type structure
α—corundum type structure
β—beta gallia type structure
K—kappa alumina type structure
u—unknown type structure similar to kappa alumina
ss—solid solution

(e) Binary oxide systems containing Sc^{+3} and larger cations.
(f) Binary oxide systems containing In^{+3} and larger cations. The Eu_2O_3–In_2O_3 system to be published [23].
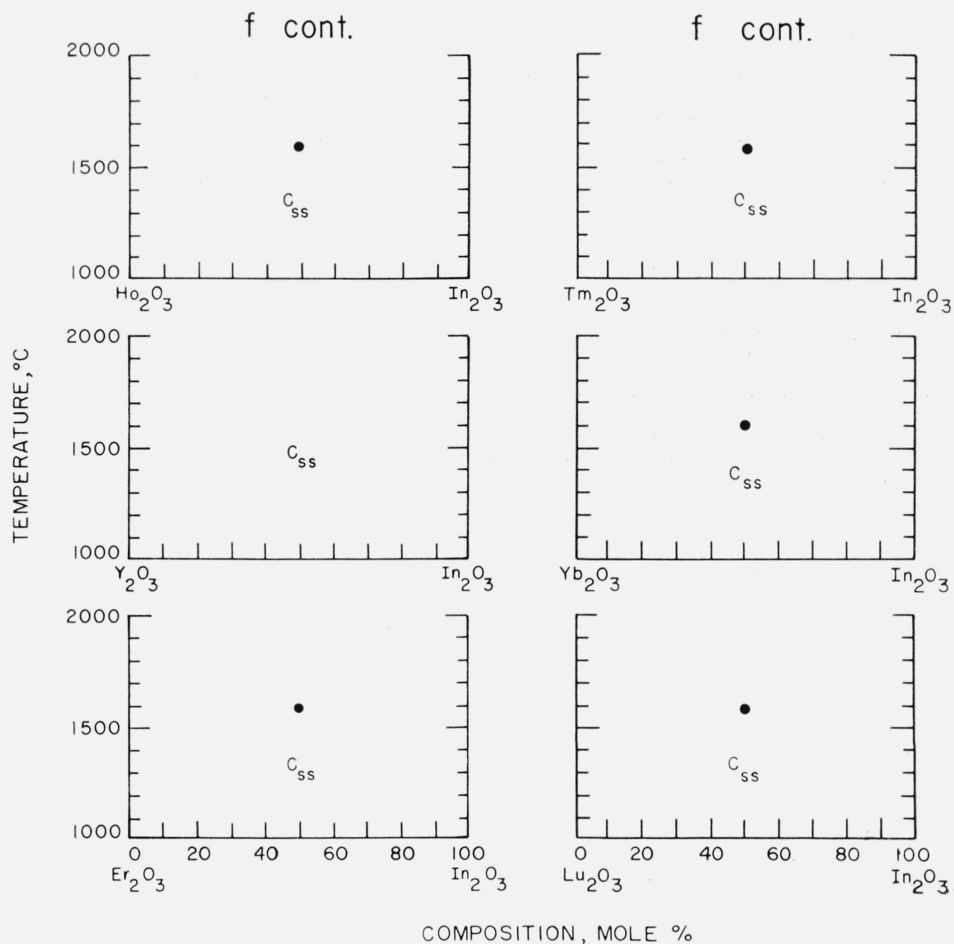
FIGURE 5. *Predicted subsolidus binary phase diagram for systems involving oxides of the trivalent cations*—Continued

●—compositions studied in present work
○—data taken from literature
✕—data taken from literature for which no temperature o heat treatment is
      given

A—A-type rare earth oxide structure
B—B-type rare earth oxide structure
C—C-type rare earth oxide structure
G—garnet type compound
11—beta alumina type structure
P—perovskite type compound
R—unknown type structure, rhombohedral symmetry

S—spinel type structure
α—corundum type structure
β—beta gallia type structure
K—kappa alumina type structure
u—unknown type structure similar to kappa alumina
ss—solid solution

(f) Binary oxide systems containing In^{+3} and larger cations.   The Eu_2O_3–In_2O_3 system to be published [23].

6. References

[1] S. J. Schneider and R. S. Roth, J. Research NBS **64A**, 317–332 (1960).

[2] V. M. Goldschmidt, T. Barth, G. Lunde, and W. Zachariasen, Pt. VII Skrifter Norske Videnskaps-Akad.   Oslo I. Mat-Naturv. K1 No. 2 (1926).

[3] M. L. Keith and R. Roy, Amer. Min. **39**, 1–23 (1954).

[4] R. S. Roth, J. Research NBS **58**, 75–88 (1957).

[5] S. Geller and E. A. Wood, Acta Cryst. **9**, 563–568 (1956).

[6] S. Geller, Acta Cryst. **10**, 243–248 (1957).

[7] S. Geller and V. B. Bala, Acta Cryst. **9**, 1019–1025 (1956).

[8] L. H. Ahrens, Geochim. et Cosmochim. Acta **2**, 155–169 (1952).

[9] R. S. Roth and S. J. Schneider, J. Research NBS **64A**, 309–316 (1960).

[10] A. Muan and S. Somiya, J. Am. Ceram. Soc. **42**, 603–613 (1959).

[11] E. Mooser and W. B. Pearson, Acta Cryst. **12**, 1015–1022 (1959).

[12] L. Pauling, The Nature of the Chemical Bond, 3d ed., Ithaca, N.Y., Cornell Univer. Press 98 (1960).

[13] W. Gordy and W. J. Orville, J. Chem. Phys. **24**, 439–444 (1956).

[14] M. W. Shafer and R. Roy, J. Am. Ceram. Soc. **42**, 563–570 (1959).

[15] R. Roy, V. G. Hill, and E. F. Osborn, Ind. and Eng. Chem. **45**, 819–820 (1953).

[16] J. A. W. Dalziel, J. Chem. Soc. Jun., 1993–1998 (1959).

[17] S. Geller and C. E. Miller, Acta Cryst. **13**, 179–186 (1960).

[18] H. J. Van Hook, J. Am. Ceram. Soc. **44**, 208–214 (1961).

[19] A. S. Russell, W. H. Gitzen, J. W. Newsome, R. W. Ricker, V. W. Stowe, H. E. Stumpf, J. R. Wall, and P. Wallace, Tech. Paper No. 10, Aluminum Co. of Amer. 1–65 (1956).

[20] H. M. Richardson, F. Ball, and G. R. Rigby, Trans. Intern. Cer. Congr., 3d Congr., Paris 173–181 (1954).

[21] E. A. Wood, Acta Cryst. **13,** 682 (1960).

[22] I. Warshaw and R. Roy, J. Am. Ceram. Soc. **42,** 434–438 (1959).

[23] S. J. Schneider, to be published in J. Research NBS **65A**, No. 5 (Sept–Oct 1961

[24] V. M. Goldschmidt, F. Ulrich, and T. Barth, Pt IV Skrifter Norske Videnskaps-Akad. Oslo I. Mat. Naturv. K1 No. 5 (1925).

[25] H. C. Stumpf, A. S. Russell, J. W. Newsome, and C. M. Tucker, Ind. and Eng. Chem. **42, 1398–1403** (1950).

[26] E. N. Bunting, NBS J. Res. **6,** 947–949 (1931).

[27] V. G. Hill, R. Roy, and E. F. Osborn, J. Am. Ceram. Soc. **35,** 135–142 (1952).

[28] V. M. Goldschmidt, T. Barth, and G. Lunde, Pt V, Skrifter Norske Videnskaps-Akad. Oslo I. Mat. Naturv. K1 No. 7 (1925).

[29] V. L. Moruzzi and M. W. Shafer, J. Am. Ceram. Soc. **4:** 367–372 (1960).

[30] J. Cassedanne and H. Forestier, Compt. Rend. **250,** 2898 2900 (1960).

[31] R. S. Roth and S. Hasko, J. Am. Ceram. Soc. **41,** 14 (1958).

[32] I. Warshaw and R. Roy, Abstract Bull. Am. Ceram Soc. **4,** 169 (1959).
Also: Presentation of paper, 61st Ann. Meet. Am Ceram. Soc., Chicago, May 19 (1959).

[33] H. S. Yoder and M. L. Keith, Am. Min. **36,** 519–53

[34] F. Bertaut and F. Forrat, Compt. Rend. **244,** 96–9 (1957).

[35] J. P. Remeika, Suppl. J. Appl. Phys. **315,** 263–264 (1960)

(Paper 65A4—116

374